Journal Pre-proof

New High-throughput Screen Identifies Compounds That Reduce Viability Specifically In Liver Cancer Cells That Express High Levels of SALL4 by Inhibiting Oxidative Phosphorylation

Justin L. Tan, Feng Li, Joanna Z. Yeo, Kol Jia Yong, Mahmoud A. Bassal, Guo Hao Ng, May Yin Lee, Chung Yan Leong, Hong Kee Tan, Chan-shuo Wu, Bee Hui Liu, Tim H. Chan, Zi Hui Tan, Yun Shen Chan, Siyu Wang, Zhi Han Lim, Tan Boon Toh, Lissa Hooi, Kia Ngee Low, Siming Ma, Nikki R. Kong, Alicia J. Stein, Yue Wu, Matan T. Thangavelu, Atsushi Suzuki, Giridharan Periyasamy, John M. Asara, Yock Young Dan, Glenn K. Bonney, Edward K. Chow, Guo-Dong Lu, Huck Hui Ng, Yoganathan Kanagasundaram, Siew Bee Ng, Wai Leong Tam, Daniel G. Tenen, Li Chai

PII: S0016-5085(19)41242-0
DOI: https://doi.org/10.1053/j.gastro.2019.08.022
Reference: YGAST 62849

To appear in: *Gastroenterology*
Accepted Date: 9 August 2019

Please cite this article as: Tan JL, Li F, Yeo JZ, Yong KJ, Bassal MA, Ng GH, Lee MY, Leong CY, Tan HK, Wu C-s, Liu BH, Chan TH, Tan ZH, Chan YS, Wang S, Lim ZH, Toh TB, Hooi L, Low KN, Ma S, Kong NR, Stein AJ, Wu Y, Thangavelu MT, Suzuki A, Periyasamy G, Asara JM, Dan YY, Bonney GK, Chow EK, Lu G-D, Ng HH, Kanagasundaram Y, Ng SB, Tam WL, Tenen DG, Chai L, New High-throughput Screen Identifies Compounds That Reduce Viability Specifically In Liver Cancer Cells That Express High Levels of SALL4 by Inhibiting Oxidative Phosphorylation, *Gastroenterology* (2019), doi: https://doi.org/10.1053/j.gastro.2019.08.022.

Chemical Genetic Screen for SALL4-expressing Cancer Dependencies

Cell A
SALL4-low

Cell B
SALL4-high

Cell A
Empty Vector

Cell A
Tg:SALL4

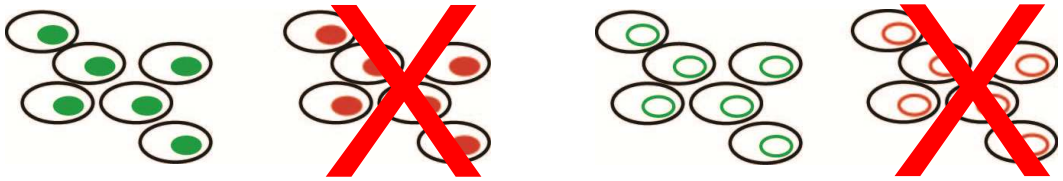

Small Molecule &
Natural Product
Cell Viability Screen

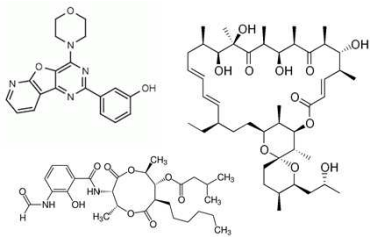

OXPHOS inhibitors

Mechanism in Cancer

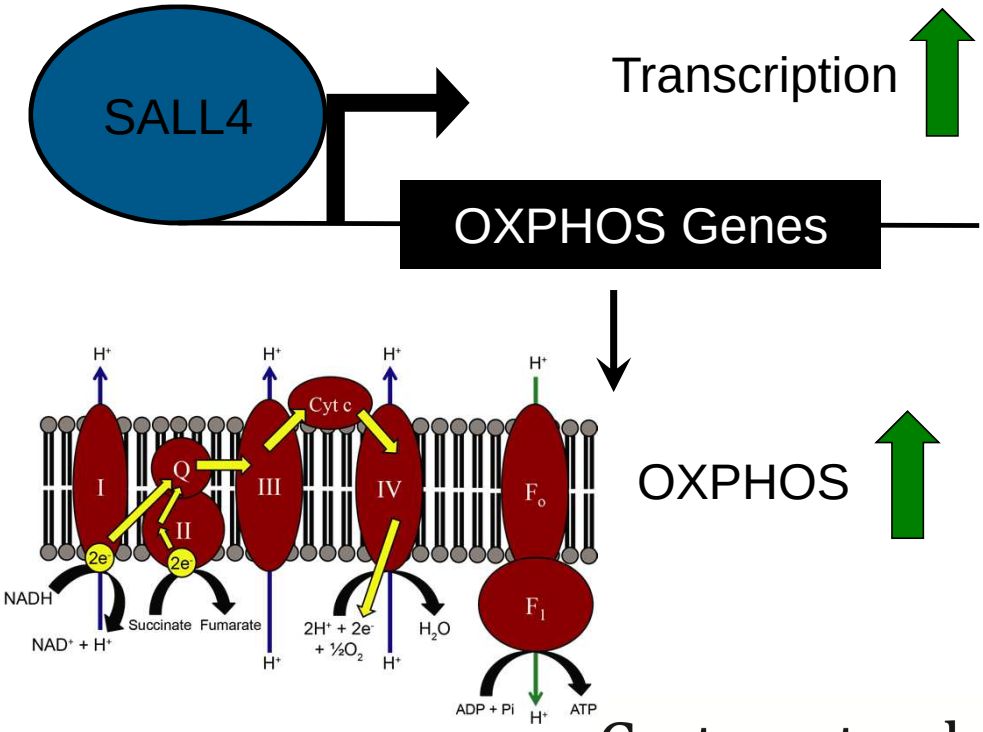

Gastroenterology

Title: New High-throughput Screen Identifies Compounds That Reduce Viability Specifically In Liver Cancer Cells That Express High Levels of SALL4 by Inhibiting Oxidative Phosphorylation

Short Title: SALL4-induced vulnerabilities in cancer

Authors: Justin L. Tan[1,2], **Feng Li**[1], Joanna Z. Yeo[1,2], Kol Jia Yong[1], Mahmoud A. Bassal[1,3,], Guo Hao Ng[2], May Yin Lee[2], Chung Yan Leong[4], Hong Kee Tan[1], Chan-shuo Wu[1], Bee Hui Liu[1], Tim H. Chan[1], Zi Hui Tan[1], Yun Shen Chan[2], Siyu Wang[2], Zhi Han Lim[2], Tan Boon Toh[1], Lissa Hooi[1], Kia Ngee Low[4], Siming Ma[2], Nikki R. Kong[5], Alicia J. Stein[5], Yue Wu[5,6], Matan T. Thangavelu[2], Atsushi Suzuki[7], Giridharan Periyasamy[2], John M. Asara[8], Yock Young Dan[1,9,10], Glenn K. Bonney[11,12], Edward K. Chow[1,13], Guo-Dong Lu[1,14,15], Huck Hui Ng[2], Yoganathan Kanagasundaram[4], Siew Bee Ng[4], Wai Leong Tam[1,2,16,17†], Daniel G. Tenen[1,3,†] & Li Chai[5†].

Author names in bold designate shared co-first authorship.

[†]Equal contribution.

Affiliations:

[1]Cancer Science Institute of Singapore, National University of Singapore, 14 Medical Drive, Singapore 117599, Singapore.

[2]Genome Institute of Singapore, Agency for Science, Technology and Research (A*STAR), 60 Biopolis Street, Singapore 138672, Singapore.

[3]Harvard Stem Cell Institute, Harvard Medical School, Boston, MA 02115, USA.

[4]Bioinformatics Institute, Agency for Science, Technology and Research (A*STAR), 30 Biopolis St, 138671, Singapore.

[5]Department of Pathology, Brigham & Women's Hospital, Harvard Medical School, Boston, MA 02115, USA.

[6]Department of Clinical Laboratory, National Cancer Center/Cancer Hospital, Chinese Academy of Medical Sciences and Peking Union Medical College, Beijing, 100021, China

[7]Division of Organogenesis and Regeneration, Medical Institute of Bioregulation, Kyushu University, 3-1-1 Maidashi, Higashi-ku, Fukuoka 812-8582, Japan.

[8]Department of Medicine, Division of Signal Transduction, Beth Israel Deaconess Medical Center and Harvard Medical School, Boston, MA 02215, USA.

[9]Department of Medicine, Yong Loo Lin School of Medicine, National University of Singapore, Singapore 119228, Singapore.

[10]Division of Gastroenterology & Hepatology, University Medicine Cluster, National University Health System, Singapore 119228, Singapore.

[11]Department of Hepatobiliary, Pancreatic Surgery and Liver Transplantation, Department of Surgery, University Surgical Cluster, National University Health System, Singapore 119228, Singapore.

[12]National University Centre for Organ Transplantation, National University Hospital, Singapore 119074, Singapore.

[13]Department of Pharmacology, Yong Loo Lin School of Medicine, National University of Singapore, Singapore 117597, Singapore.

[14]Department of Toxicology, School of Public Health, Guangxi Medical University, Nanning 530021, China.

[15]Key Laboratory of High-incidence-Tumor Prevention & Treatment (Guangxi Medical University), Ministry of Education of China, Nanning 530021, China.

[16]Department of Biochemistry, Yong Loo Lin School of Medicine, National University of Singapore, Singapore 117597, Singapore.

[17]School of Biological Sciences, Nanyang Technological University, 60 Nanyang Drive, Singapore 637551, Singapore.

Grant support: This work was supported by the Genome Institute of Singapore Innovation Fellow Award (J.L.T.); A*STAR A*ccelerate Gap Funding ETPL/18-GAP018-R20H (J.L.T.); Singapore Ministry of Health's National Medical Research Council (Singapore Translational Research (STaR) Investigator Award, D.G.T.; NMRC/OFIRG/0064/2017, W.L.T; LCG17MAY004, W.L.T.; NMRC/TCR/015-NCC/2016, W.L.T.); National Research Foundation Singapore (NRF-NRFF2015-04 Grant, W.L.T.) and the Singapore Ministry of Education under its Research Centres of Excellence initiative; Singapore Ministry of Education Academic Research Fund Tier 3, grant number MOE2014-T3-1-006 (D.G.T); NIH/NCI Grant R35CA197697 (D.G.T); NIH/NHLBI Grant P01HL095489 (L.C.); LLS Grant P-TRP-5854-15 (L.C). This work was supported in part by the JSPS KAKENHI (Grant Numbers: JP17H05623, JP17K19603, JP18H05102, JP19H01177, and JP19H05267) (A.S.).

Correspondence to: daniel.tenen@nus.edu.sg, lchai@bwh.harvard.edu, tamwl@gis.a-star.edu.sg

Disclosures: J.L.T., Y.K., S.B.N., W.L.T., L.C., and D.G.T. are co-inventors on a patent application filed by A*STAR A*ccelerate, the National University of Singapore, and Brigham & Women's Hospital relating to work in this manuscript.

Data and materials availability: All sequencing data have been deposited in the NCBI Gene Expression Omnibus databases GSE114808 and GSE112729.

To review GEO accession GSE112729:
Go to https://www.ncbi.nlm.nih.gov/geo/query/acc.cgi?acc=GSE112729
Enter token gdyfgeoapjevdql into the box

To review GEO accession GSE114808:
Go to https://www.ncbi.nlm.nih.gov/geo/query/acc.cgi?acc=GSE114808
Enter token ajudymeanhstnqd into the box

Author contributions: J.L.T. conceptualized the project and wrote the manuscript. J.L.T., L.F. and J.Z.Y. participated in data curation, methodology and investigation; Y.K. and S.B.N. participated in investigation and provided resources; J.L.T., D.G.T, W.L.T. and L.C. provided supervision and resources; all other authors participated in data curation and investigation.

Acknowledgments: We thank Min Yuan for her assistance with the metabolite profiling experiments.

Abstract:

Background and Aims: Some oncogenes encode transcription factors, but few drugs have been successfully developed to block their activity specifically in cancer cells. The transcription factor SALL4 is aberrantly expressed in solid tumor and leukemia cells. We developed a screen to identify compounds that reduce the viability of liver cancer cells that express high levels of SALL4 and we investigated their mechanisms.

Methods: We developed a stringent high-throughput screening platform comprising unmodified SNU-387 and SNU-398 liver cancer cell lines and SNU-387 cell lines engineered to express low and high levels of SALL4. We screened 1597 pharmacologically active small molecules and 21,575 natural product extracts from plant, bacteria, and fungal sources for those that selectively reduce the viability of cells with high levels of SALL4 ($SALL4^{hi}$ cells). We compared gene expression patterns of $SALL4^{hi}$ cells vs SALL4-knockdown cells using RNA-seq and real-time PCR analyses. Xenograft tumors were grown in NOD/SCID gamma mice from $SALL4^{hi}$ SNU-398 or HCC26.1 cells or from $SALL4^{lo}$ PDX cells; mice were given injections of identified compounds or sorafenib and the effects on tumor growth were measured.

Results: Our screen identified 1 small molecule (PI-103) and 4 natural compound analogues (oligomycin, efrapeptin, antimycin, and leucinostatin) that selectively reduced viability of $SALL4^{hi}$ cells. We performed validation studies, and 4 of these compounds were found to inhibit oxidative phosphorylation. The ATP synthase inhibitor oligomycin reduced the viability of $SALL4^{hi}$ hepatocellular carcinoma and non-small–cell lung cancer cell lines with minimal effects on $SALL4^{lo}$ cells. Oligomycin also reduced the growth of xenograft tumors grown from $SALL4^{hi}$ SNU-398 or HCC26.1 cells, to a greater extent than sorafenib, but oligomycin had little effect on tumors grown from $SALL4^{lo}$ PDX cells. Oligomycin was not toxic to mice. Analyses of chromatin immunoprecipitation sequencing data revealed that SALL4 binds approximately 50% of mitochondrial genes, including many oxidative phosphorylation genes, to activate their transcription. In comparing $SALL4^{hi}$ and SALL4-knockdown cells, we found SALL4 to increase oxidative phosphorylation, oxygen consumption rate, mitochondrial membrane potential, and utilization of oxidative phosphorylation-related metabolites to generate ATP.

Conclusions: In a screen for compounds that reduce the viability of cells that express high levels of the transcription factor SALL4, we identified inhibitors of oxidative phosphorylation, which slowed the growth of xenograft tumors from $SALL4^{hi}$ cells in mice. SALL4 activates transcription of genes that regulate oxidative phosphorylation to increase oxygen consumption, mitochondrial membrane potential, and ATP generation in cancer cells. Inhibitors of oxidative phosphorylation might be used for treatment of liver tumors with high levels of SALL4.

Keywords: chemical genetic screen; HCC; metabolic vulnerability; metabolism

Introduction

Transcription factors are the second largest class of oncogenes[1]. However, the molecular mechanisms by which these transcription factors exert their cancer-driving effects are not well understood. There is renewed interest in phenotypic cell-based screens for studying the underlying mechanisms of various diseases, aiding in subsequent drug discovery[2]. Common methods for cell-based drug discovery include the screening of endogenous cell lines with and without the gene or mutation of interest, or the use of isogenic cell line systems in which the gene of interest is altered or expressed in an unaffected cell to control for genetic background[2,3]. In both endogenous and isogenic systems, hits are defined by their ability to selectively target cells expressing the alteration of interest, while not affecting the control cells. The disadvantage of the endogenous system is that cell lines are genetically distinct, so hits obtained may target pathways unrelated to the alteration of interest[2]. The isogenic system avoids the genetic complexity of the endogenous system, but suffers the drawback of compound interference with the transgene, resulting in hits that might not be biologically relevant[4]. To overcome these drawbacks, we developed a screening platform that encompasses both endogenous and isogenic methodologies, applying the platform to identify vulnerabilities induced by oncogene SALL4 mis-expression in hepatocellular carcinoma (HCC).

Liver cancer is the sixth most common cancer but is the second leading cause of cancer deaths worldwide owing to limited therapeutic interventions[5]. HCC is the predominant subtype of liver cancer, with 85% of liver cancer patients suffering from HCC. The only approved targeted therapies for treating HCC, kinase inhibitors sorafenib and regorafenib, target tumor vasculature, but they are largely ineffective and are used as a last resort[6,7]. There is an increased urgency to discover precision medicine interventions for this unmet need.

SALL4 (*Spalt*-like transcription factor 4) is an oncofetal protein essential for self-renewal and maintaining pluripotency in embryonic stem cells, and it plays a critical role in early embryonic development[8–11]. It is subsequently silenced in most adult tissues, but aberrantly re-expressed to drive tumorigenesis in various cancers[9,12]. *SALL4* is highly expressed in fetal liver but is silenced in the adult liver[13], and often reactivated in HCC, in which 30-50% of tumours show significant *SALL4* expression[14]. There are two isoforms of *SALL4* (*SALL4A* and *SALL4B*) that have overlapping but non-identical binding regions in the genome, and *SALL4B* alone can maintain pluripotency[15]. Both isoforms are derived from the same transcript, where SALL4A is the full length spliceoform and SALL4B lacks part of exon 2[9,16]. It has been observed that both *SALL4* isoforms are co-expressed when *SALL4* is transcriptionally upregulated[14]. *SALL4* is a C2H2 zinc-finger transcription factor that can act as a transcriptional activator or repressor[15,17,18]. The repressive function of SALL4 is achieved through recruitment of the Nucleosome Remodelling and Deacetylase complex (NuRD)[19]. In cancer, SALL4 recruits NuRD to genes such as the *PTEN* tumour suppressor, deacetylating and silencing the locus[19]. The transcriptional activation function of SALL4 also plays a role in cancer. SALL4 has been shown to transcriptionally activate the *c-MYC* oncogene in endometrial cancer[20] and HOXA9 in acute myeloid leukemia[21]. The *in vivo* tumorigenic potential of SALL4 is reflected in a mouse model of constitutive *SALL4B* expression, which results in the onset of acute myeloid leukemia (AML) and HCC[22]. Therapeutic interventions that target SALL4 and its dependencies remain elusive.

Here, we developed a screening platform that encompasses both endogenous and isogenic methodologies, applying the platform to discover drugs targeting oncogene SALL4-induced dependencies in hepatocellular carcinoma (HCC). Our platform utilizes an endogenous pair of

SALL4-expressing ($SALL4^{hi}$) and SALL4 undetectable ($SALL4^{lo}$) HCC cell lines, as well as isogenic SALL4 undetectable cell lines engineered to express SALL4 isoforms. We screened both synthetic and diverse natural product extract libraries to identify hit compounds that specifically decrease $SALL4^{hi}$ cell viability. Unexpectedly, our screen identified 4 oxidative phosphorylation inhibitors as being selective for $SALL4^{hi}$ cells. Our most potent and selective compound, ATP synthase inhibitor oligomycin, can selectively target a panel of $SALL4^{hi}$ HCC and lung cancer cell lines, over $SALL4^{lo}$ cells. Oligomycin also demonstrates similar *in vivo* tumor suppressive activity as HCC standard-of-care drug sorafenib, but at a 200 times lower dose. This *in vivo* efficacy is only observed in SALL4-high and not SALL4-low tumors. Analysis of SALL4 ChIP-seq data revealed SALL4 binding to a significant number of oxidative phosphorylation genes in $SALL4^{hi}$ HCC. SALL4 predominantly upregulates expression of these genes, as revealed by RNA-seq, mRNA expression and protein analyses. SALL4 expression functionally increases oxidative phosphorylation, as measured by cellular oxygen consumption rate, and supported by imaging and metabolite profiling. Our work demonstrates the ability of our endogenous-isogenic combination cell-based screening methodology to successfully identify a metabolic pathway vulnerability, which is therapeutically actionable with a good therapeutic index, in SALL4-expressing cancers.

Materials and Methods

Chemical genetic screen

SNU-387 empty vector, *Tg:SALL4A*, and *Tg:SALL4B* expressing isogenic cell lines were generated by transducing WT SNU-387 cells with empty vector, SALL4A or SALL4B FUW-Luc-mCh-puro lentiviral constructs[20]. Cells were plated in 50 µl of RPMI culture media in 384-well white flat-bottom plates (Corning) and incubated at 37°C in a humidified atmosphere of 5% CO_2 overnight. Cell numbers per well were 1500 for SNU-398, and 750 for SNU-387 and SNU-387 isogenic lines. After overnight incubation, 0.5 µl of 100 µM drug libraries or 10 mg/ml extract libraries were added to cells with the Bravo Automated Liquid Handling Platform (Agilent). Cells were then incubated for 72 hrs at 37°C in a humidified atmosphere of 5% CO_2 before 10 µl of CellTiter-Glo reagent was added to the wells with the MultiFlo Microplate Dispenser (BioTek). Cells were incubated at room temperature for a minimum of 10 minutes after which luminescence readings were recorded by an Infinite M1000 Microplate Reader (Tecan).

HCC sample collection

The collection of HCC samples from HCC patients for research is performed under Domain Specific Review Board (DSRB) protocol 2011/01580 approved by the National Healthcare Group DSRB, which governs research ethics in Singapore that involves patients, staff, premises or facilities of the National Healthcare Group as well as any other institutions under its oversight.

Results

An endogenous-isogenic chemical genetic screening platform identifies SALL4-selective compounds

Our SALL4-dependent chemical-genetic screening platform consists of a pair of endogenous HCC cell lines and a trio of isogenic cell lines (Fig. 1A). For the endogenous pair, SNU-398 expresses high levels of SALL4 protein, and its survival is dependent on *SALL4* expression[14]. The endogenous control SNU-387 cell line has undetectable *SALL4* RNA (Fig. S1A) and protein. The isogenic trio consists of lentiviral-mediated insertions into the SNU-387 SALL4 undetectable line, in which the cells are transduced with either an empty vector control, or a *SALL4A* or *SALL4B* expressing construct (Fig. 1A). The *SALL4* expressing isogenic lines demonstrate SALL4 isoform-specific mRNA and protein expression (Fig. S1B, S1C and S1D) and become sensitive to *SALL4* knockdown (Fig. S1D and S1E). SALL4 isoform expression in these isogenic cells does not alter their growth and proliferation rates (Fig. S1F and S1G).

The five endogenous and isogenic cell lines were screened with 1,597 pharmacologically active small molecules from the Selleck Anti-cancer and LOPAC1280 libraries, and 21,575 diverse natural product extracts of plant, fungal, and actinobacteria origin from the A*STAR Bioinformatics Institute collection[23]. Each natural product extract contains varying numbers of compounds, allowing multiplexing to achieve a screen with hundreds of thousands to millions of compounds efficiently. Cell viability was assessed after 72 hrs of compound or extract incubation (Fig. 1A). Extracts and compounds that reduced cell viability of the SALL4^{hi} cell lines (SNU-398, SNU-387 *Tg:SALL4A* and *Tg:SALL4B*) by more than 1.5-fold but had minimal effect on SALL4^{lo} (SNU-387, and SNU-387 Empty Vector) cell viability were identified as hits. The controls for the screen were proteasome inhibitor bortezomib, which significantly reduced cell viability of all cell lines, and the sole hit from the small molecule library screen, PI-103, which selectively targets the SALL4^{hi} cells (Fig. S2A). The Z-factor of the screen was between 0.70 and 0.86.

We obtained three categories of hits from the screen: compounds/extracts that selectively targeted endogenous SALL4^{hi} SNU-398 over SALL4^{lo} control SNU-387 (117 hits), compounds/extracts that selectively targeted *Tg:SALL4A* cells over Empty Vector control (420 hits), and compounds/extracts that selectively targeted *Tg:SALL4B* cells over control (960 hits) (Fig. 1B). Each category gave at least 100 hits but taken together, the overlapping results gave only 17 hits (1 small molecule and 16 natural product extract hits). Our combined screening methodology yields a small number of hits that conform to stringent SALL4-specificity requirements, decreasing the time and cost for further validation and work-up of hits.

Since each natural product extract we screened is a mixture of compounds, we determined the specific active components responsible for the SALL4^{hi} response. 31 natural product extract hits from the Tg:SALL4A-SNU-398 overlap (3 hits), Tg:SALL4B-SNU-398 overlap (12 hits), and all three cell line overlap (16 hits) were retested in the screening assay, and only 18 were reproducible (Fig. 1C). These 18 hits were then validated with dose response curves, where only 12 hits from the all three cell line overlap category were validated (Fig. 1C). No hits from the Tg:SALL4A-SNU-398 or Tg:SALL4B-SNU-398 categories passed through this validation step. Next, we fractionated the 12 validated hit extracts into 38 fractions each. Fractions were then screened to identify 9 discrete fractions that were selective for SALL4-high cells, and positive fractions were subjected to Q-TOF mass spectrometry and nuclear magnetic resonance analysis to identify active components (Fig. 1C).

Oxidative phosphorylation inhibitors target SALL4-dependent cell viability

Overall, the screen identified one small molecule hit, PI-103, and 4 natural compound analogues of oligomycin, efrapeptin, antimycin, and leucinostatin as being selective for SALL4^{hi} cells (Fig. 2A and S2A), with a hit rate of 0.02%. Oligomycin and leucinostatin are known inhibitors of the F_0 ATP synthase subunit, efrapeptin inhibits the F_1 ATP synthase subunit, and antimycin targets cytochrome c reductase in Complex III of oxidative phosphorylation[24,25] (Fig. 2B). PI-103 has been shown to induce mitochondrial apoptosis in acute myeloid leukemia cells[26]. Since the CellTiter-Glo reagent we used for the screen quantifies ATP levels as a measure of cell viability, and our hits target oxidative phosphorylation and the mitochondria, which is a major source of cellular ATP, we further validated our hits with the CyQUANT DNA dye as an alternative measure of cell viability. The dose response curves for the 5 hits using either CellTiter-Glo or CyQUANT were highly comparable (Fig. S2B and S2C). We also tested various analogues of oligomycin and efrapeptin in our cell-based assay (Table S1A). The 4 natural compounds and their analogues demonstrated potent IC_{50} values in the 0.1 to 10 nM range for the endogenous SALL4^{hi} SNU-398 line and partial cell viability decreases in the SALL4^{hi} isogenic lines, with selectivity ratios ranging from 200 to 20,000 fold compared to the IC_{50} values in the SALL4^{lo} control cells (Fig. 1A and S1C, Table S1A). In SALL4-high cells, oligomycin A seems to induce cell death through apoptosis, as suggested by the presence of cleaved caspase-3 with oligomycin treatment in a dose response manner (Fig. S2D).

Oligomycin A suppresses SALL4-dependent tumorigenesis

We selected oligomycin A for downstream tumor-suppression and mechanistic studies since it had the most potent SALL4^{hi} cell IC_{50} of 0.5 nM and the highest selectivity of 20,000 fold over the SALL4^{lo} cells. Oligomycin A is also readily available commercially. To determine if oligomycin A could selectively target other SALL4^{hi} cell lines, we performed dose response cell viability experiments on a panel of HCC cell lines. This panel includes two patient-derived primary cell lines, HCC9.2 and HCC26.1, from two Singapore HCC cases, and an immortalized normal liver cell line THLE-3 (Fig. 3A and S3A). We also tested oligomycin A in a pair of non-small cell lung cancer (NSCLC) cell lines, in which the SALL4^{hi} H661 line was previously shown to be dependent on SALL4 expression, while the SALL4^{lo} H1299 line was not[27] (Fig. S3B and S3C, Table S1B). Our data suggests that oligomycin A is potent and selective against SALL4^{hi} expressing HCC and NSCLC cell lines (Fig. 3A and S3A-C, Table S1A and B).

To test the *in vivo* efficacy of oligomycin A in suppressing HCC tumors, we utilized a SALL4-high mouse xenograft model of SALL4-dependent SNU-398 cells, a SALL4-high patient-derived xenograft model derived from the HCC26.1 patient primary cell line expressing high levels of SALL4 (Fig. S3A), and a SALL4-low patient-derived xenograft model of a tumor named PDX1. In the SALL4-high SNU-398 cell line model, oligomycin A was able to suppress tumor size to a similar degree to the standard-of-care drug in HCC, sorafenib, but at a 200 times lower dose of 0.1 mg/kg compared to 20 mg/kg for sorafenib (Fig. 3B, 3C and S3D). Similarly, oligomycin A or sorafenib treatment was able to suppress tumors in our SALL4-high PDX model with tumor suppression synergy observed in the sorafenib-oligomycin combination treatment (Fig. 3D, 3E and S3E). The PDX1 tumors, which showed very low SALL4 protein levels (Fig. S3F), did not respond to oligomycin treatment (Fig. 3F, 3G and S3G). Mouse weight was not significantly affected by oligomycin treatment in all models (Fig. 3H-J). We examined the known oligomycin side effects of muscle weakness, respiratory depression, and convulsions[28,29] in mice treated with vehicle or oligomycin over 3 weeks. To assess muscle weakness, we carried out the open field test, grip strength test, and rotarod test. In the open field

test, the distance travelled by the mice in 30 mins was not significantly affected, while their average velocity of movement was slightly decreased with oligomycin treatment (Fig. S3H). In the grip strength test, the normalized full body force was not significantly affected, while the forepaw force was slightly decreased with oligomycin treatment (Fig. S3I). In the rotarod test, the latency to fall of the mice was not significantly affected by oligomycin treatment (Fig. S3J). We did not observe any respiratory depression or convulsions in the mice. Our data suggest that the drug was not highly toxic to the mice at this therapeutic dose.

To examine a potential correlation of oxidative phosphorylation inhibition in patients, we re-examined a HCC patient dataset that we previously published for SALL4 expression[14,30]. The first-line treatment for Type II diabetes is the biguanide drug metformin, which has been shown to inhibit oxidative phosphorylation[31,32]. We previously observed that 60% of HCC patient tumors had detectable levels of SALL4, but when we stratified patients with and without diabetes, we noticed a significant difference (Fig. S3K). Non-diabetic patients showed the same trend of 60% SALL4 positivity as all patients combined, however, the trend was reversed in diabetic patients with only 40% having SALL4 positive tumors (Fig. S3K). Patient information on the type of diabetes and metformin use is unavailable so more clinical work is needed to validate this correlation. We tested phenformin, an analogue of metformin with known oxidative phosphorylation inhibition activity[32], in our SALL4 isogenic cell lines. We observed partial sensitivity to phenformin in the SALL4-expressing cells compared to the parental SALL4 low line, but the effect was not as prominent as that of oligomycin A (Fig. S3L). The lower effectiveness of phenformin is expected since it is a less potent inhibitor of oxidative phosphorylation (mM IC_{50})[32] compared to oligomycin A (nM IC_{50})[33]. Our data suggests the possibility that oxidative phosphorylation inhibition by metformin treatment in diabetic patients suppresses SALL4-positive tumorigenesis.

Oncogenic SALL4 binds oxidative phosphorylation genes and predominantly upregulates them

Since the hits from our screen predominantly target oxidative phosphorylation, we examined our previous SALL4 and acetylated H3K27 chromatin immunoprecipication sequencing (ChIP-seq) data in the SNU-398 cells[34]. We found that SALL4 binds up to 45% of mitochondrial genes, as defined by the MitoCarta 2.0 gene list, and gene ontology analysis revealed that a significant number of these genes are involved in oxidative phosphorylation (Fig. 4A, Table S2). Gene meta analysis of SALL4 and H3K27ac occupancy at these mitochondrial genes revealed that SALL4 binds predominantly at the promoter region, between the H3K27ac double peaks[35] (Fig. 4B and 4C).

To assess gene expression changes caused by SALL4 activity, we performed RNA-seq on the isogenic *SALL4* expressing cells and SNU-398 SALL4-high cells with *SALL4* knockdown (Fig. S4A). We observed that oxidative phosphorylation and other mitochondrial genes with SALL4-bound promoters show increased mRNA expression with *SALL4* expression, particularly with the *SALL4B* isoform (Fig. 4D). In addition, *SALL4* knockdown downregulates the expression of these genes (Fig. S4B). We validated the observed RNA-seq expression patterns of some of these genes by qRT-PCR (Fig. S4C and S4D). Gene Set Enrichment Analysis (GSEA)[36] of the RNA-seq data revealed significant enrichment of oxidative phosphorylation genes in the SNU-398 control compared to *SALL4* knockdown, and in the SALL4B expressing isogenic cell line compared to empty vector control (Fig. S4E, Table S3A-F). This suggests that the binding of

SALL4, to oxidative phosphorylation and other mitochondrial gene promoters, predominantly activates transcription of these genes. Genes that are not bound by SALL4 such as *SUMO1* are unaffected (Fig. 4C, 4D and S4B). Western blots of SALL4-bound oxidative phosphorylation genes ATP5D, ATP5E, ATP5G2, and NDUFA3, and other SALL4-bound mitochondrial genes ARG2, MRPL24, and SLC25A23, show similar trends in gene expression data, in which *SALL4* expression (predominantly *SALL4B*) upregulates their protein levels while *SALL4* knockdown downregulates these levels (Fig. 4E, 4F, S4F and S4G).

SALL4 expression functionally increases oxidative phosphorylation

Since SALL4 expression in our HCC cell lines enhances oxidative phosphorylation gene mRNA and protein expression, we examined if these changes would result in functional alterations in oxidative phosphorylation. We first measured the oxygen consumption rate (OCR) of the SALL4^{hi} and SALL4^{lo} cells used in the screen, since oxidative phosphorylation requires oxygen. We observed that the OCR is significantly increased in the SNU-398 SALL4^{hi} line and by expressing either *SALL4A* or *SALL4B* in the isogenic lines (Fig. 5A). The opposite occurs with *SALL4* knockdown in SNU-398 cells, in which OCR decreases proportionally with decreasing SALL4 protein levels, as shSALL4-2 reduces SALL4 protein level to a greater degree than shSALL4-1 (Fig. 5B and S4G). This suggests that *SALL4* expression increases oxidative phosphorylation-dependent OCR.

To assess mitochondrial localization and the mitochondrial membrane potential gradient generated by oxidative phosphorylation, we performed immunofluorescence imaging of the SALL4 endogenous and isogenic cell lines with oxidative phosphorylation membrane protein Cytochrome c and MitoTracker dye, a dye which localizes to the mitochondrial membrane in a membrane potential-dependent manner (Fig. 5C). Quantification of the fluorescence signals per cell revealed that Cytochrome c is significantly upregulated in the SALL4A expressing cells (Fig. 5D). In addition, the MitoTracker signal is significantly increased in the SNU-398 and both *SALL4A* and *SALL4B* expressing cells (Fig. 5E). These results suggest that *SALL4* expression increases oxidative phosphorylation-dependent mitochondrial membrane potential.

Since oxidative phosphorylation is functionally increased by SALL4 expression, we analysed the levels of oxidative phosphorylation-related metabolites. We first measured ATP levels normalized to DNA content in the SALL4 expressing cells and found that ATP levels are significantly increased in both the *SALL4A* and *SALL4B* expressing lines (Fig. 5F). We also performed metabolite profiling on the SALL4 expressing lines and through Metabolite Set Enrichment Analysis (MSEA)[37], observed that electron transport chain (oxidative phosphorylation) and malate-aspartate shuttle metabolites are significantly altered in both *SALL4A* and *SALL4B* expression (Fig. S5A and S5B). The malate-aspartate shuttle facilitates the transfer of electrons from membrane impermeable NADH generated during glycolysis in the cytosol to mitochondrial oxidative phosphorylation[38]. NADH levels are significantly lower in the *SALL4* expressing lines while NAD+ levels are significantly higher, implying that there is an increased conversion of NADH into NAD+ by oxidative phosphorylation Complex I (Fig. 5G). Malate-aspartate shuttle metabolites are also significantly increased, suggesting an increase in the transfer of electrons (NADH) generated in glycolysis to oxidative phosphorylation (Fig. S5C). Our metabolite profiling data implies that *SALL4* expression increases the utilization of oxidative phosphorylation-related metabolites to generate more ATP.

Many cancers demonstrate the Warburg effect, where glycolysis is upregulated by the PI3K/mTOR signalling pathway[39]. Our small molecule SALL4-selective hit from the screen, PI-103, is a pan PI3K inhibitor (Fig S2A). We therefore examined the effects of SALL4 expression on glycolysis in our oxidative phosphorylation-dependent model. From our metabolite profiling data, glycolytic metabolites are primarily downregulated with SALL4 expression (Fig. S5D). The levels of L-lactate, the end product of anaerobic respiration, were unchanged with SALL4 expression (Fig. S5E). Further, we measured the extracellular acidification rate (ECAR) of the SALL4 isogenic cell lines, which measures lactate being secreted into the extracellular environment, and observed a slight decrease in the ECAR with SALL4 expression (Fig. S5F). In the glycolysis stress test, we observed a marked decrease in glycolytic rate and a slight decrease in glycolytic capacity in the SALL4 expressing cells (Fig. S5G). To ascertain if PI3K inhibition is important for SALL4-selectivity, we tested a number of PI3K isoform-specific and mTOR inhibitors in our endogenous and isogenic cell lines. However, most of these inhibitors did not recapitulate the specificity for SALL4-expressing lines observed with PI-103 treatment (Fig. S6A). The SALL4-selectivity of PI-103 could be due to an off-target effect, rather than by modulating the PI3K pathway. From these experiments, it is likely that SALL4 expression in cancer neither initiates the Warburg effect nor creates a dependency on glycolysis.

Interestingly, the top altered metabolic pathway due to SALL4 expression was the urea cycle (Fig. S5A and S5B). We observed significant upregulation of urea cycle metabolites, particularly in the SALL4B expressing cells, in our metabolite profiling data (Fig. S7A). When we examined our ChIP-seq data for urea cycle genes, we only observed SALL4 binding at the promoter region of *ARG2* (Fig. S7B). This suggests a possible coupling of oxidative phosphorylation and the urea cycle through *ARG2* regulation by SALL4. However, since SALL4 binds only one gene in the urea cycle, it is unlikely that the urea cycle plays a direct role in SALL4-dependent cancer.

We also examined mitochondrial DNA (mtDNA) copy number through qRT-PCR analysis with mtDNA gene-specific primers[40] and found that the examined mtDNA regions are significantly amplified in SNU-398 SALL4^{hi} cells and *SALL4* expressing isogenic lines (Fig. S7C). This suggests that SALL4 expression promotes an increase in mtDNA copy number in relation to increased oxidative phosphorylation functionality in the mitochondria. We also examined the expression of mitochondrial biogenesis regulators *PGC-1α*, *PGC-1β*, *TFAM*, *NRF1*, and *NRF2*[41–43], in our SALL4-expressing isogenic lines. Only *PGC-1α* was significantly upregulated in the SALL4B-expressing line while there were no appreciable alterations in *TFAM*, *NRF1*, and *NRF2* (Fig. S7D). *PGC-1β* expression was not detected in these lines. In our ChIP-seq data, SALL4 binding was only observed at the promoters of *NRF2* and *TFAM* (Fig. S7E). Our data suggests that SALL4 does not directly regulate the expression of mitochondrial biogenesis genes.

Conclusions:

A combined chemical-genetic screening to discover oncogenic transcription factor vulnerabilities as precision medicine

Our chemical genetic screening platform with endogenous and isogenic SALL4 expressing HCC cell lines allows for the efficient and stringent identification of a small number of hits that target both the endogenous and isogenic SALL4^{hi} lines, increasing the likelihood that these hits

are specifically affecting SALL4-related biology. The endogenous pair gives biological relevance while the isogenic trio controls for genetic background. Our combination endogenous-isogenic screen is therefore able to identify compounds that target SALL4-specific biology in a biologically relevant fashion. The 4 natural compound hits identified target different oxidative phosphorylation components and by doing so, they potently and selectively target *SALL4* expressing cells in both HCC and NSCLC systems. We demonstrate that ATP synthase inhibitor oligomycin A effectively targets SALL4^{hi} cells in a panel of HCC cell lines and can suppress tumors *in vivo* to a similar degree as the current standard-of-care drug sorafenib. Oligomycin and sorafenib also act in synergy to suppress tumorigenesis when combined. This suggests that our system can identify tool compounds that are specific to transcription factor cancer biology efficiently and effectively. Our proof-of-concept screen could have important implications for future academic studies of oncogenic transcription factor downstream pathways, and potential precision medicine applications.

A previously unknown metabolic role of SALL4 in tumorigenesis

From prior work, the widely accepted role of transcription factor SALL4 in cancer has been to modulate the expression of both pro- and anti-cancer genes, such as by recruiting the NuRD complex to chromatin to silence PTEN, or by directly upregulating oncogene MYC levels.

Our screening results and subsequent investigation into the altered processes in SALL4-dependent tumorigenesis reveals a previously unknown metabolic reprogramming function of SALL4. We demonstrate that SALL4 binds a significant number of oxidative phosphorylation and other mitochondrial genes at their promoters and predominantly upregulates their mRNA expression. This gene expression upregulation ultimately leads to increased protein levels of these genes. *SALL4* expression also leads to a functional increase in oxidative phosphorylation, with increased cellular OCR, mitochondrial membrane potential, oxidative phosphorylation-related metabolites and mtDNA copy number. Since SALL4 expression in our isogenic cell lines does not affect cell proliferation, we believe that oxidative phosphorylation is specifically co-opted by SALL4 mis-expression in cancer, and not as a result of increased proliferation rate upregulating non-specific housekeeping processes. Our work proposes that *SALL4* expression in cancer confers a dependency on oxidative phosphorylation through direct gene expression regulation, although the underlying preference for this metabolic reprogramming in tumorigenesis is still unclear.

We did not observe the Warburg effect, the preference for cancers to upregulate anaerobic glycolysis for energy, in our *SALL4*-expressing cancer cell models. Recent studies have challenged the hypothesis that the Warburg effect is cancer specific, suggesting that the effect is a result of metabolic changes associated with a proliferative state, rather than a unique feature of malignancy[44]. Many non-malignant cells utilize the Warburg effect to proliferate. There are many advantages of non-Warburg aerobic respiration to proliferating cells, such as the supply of large quantities of anabolic precursors such as nucleotides, proteins, and lipids. Many tumor cells have been shown to utilize the TCA cycle and oxidative phosphorylation to generate ATP and balance reactive oxygen species[45]. Tumorigenesis has also been shown to be dependent on mitochondrial function. Cancer cells can use fatty acids and amino acids, rather than glucose, to supply intermediates for the TCA cycle and maintain mitochondrial respiration, particularly during changes in the tumor microenvironment[30,46]. This might explain why SALL4-expressing

cells upregulate oxidative phosphorylation to become tumorigenic, thereby becoming sensitive to oxidative phosphorylation inhibitors, rather than demonstrating the Warburg effect.

Other than being a potent oncogene, SALL4 is an important developmental gene in the fetal liver and in stem cells. It would be interesting to determine if oxidative phosphorylation and other metabolic processes are similarly regulated by homeostatic SALL4 expression in the developing embryo or the stem cell compartment during liver regeneration post injury. The role of SALL4 in liver regeneration is poorly understood and future studies are prudent for dissecting this role in greater detail.

SALL4 as a potential biomarker for oxidative phosphorylation precision medicine in cancer

Clinical trials have been conducted to assess the effectiveness of oxidative phosphorylation inhibitors as effective cancer therapies[47]. However, the direct molecular mechanisms of oxidative phosphorylation phosphorylation upregulation in cancer are not well understood, particularly in liver cancer. This, coupled with toxicity associated with targeting a ubiquitous cellular pathway, currently make these inhibitors less appealing as cancer drugs.

Our study demonstrates the possibility of SALL4 to be used as a companion biomarker to select cancer patients who may benefit from oxidative phosphorylation inhibitors in the clinic. Mechanistically, we propose a direct link between SALL4 upregulation and an increase in oxidative phosphorylation, where SALL4 binds and transcriptionally activates oxidative phosphorylation genes during tumorigenesis. Tumors that express significant levels of SALL4 are more sensitive to oxidative phosphorylation inhibition at very low doses, as we have demonstrated both *in vitro* and *in vivo*. A larger therapeutic window for clinical oxidative phosphorylation inhibitors is therefore possible in patients harboring SALL4-expressing tumors. Targeting SALL4-dependent cancer with oxi oxidative phosphorylation inhibitors could lead to an effective suppression of tumorigenesis with minimal toxicity. The patient data we examined shows promise for precision medicine use of oxidative phosphorylation inhibitors in SALL4 patients, but the limitations of the annotated patient bio-data, the small samples size, and the low potency of biguanides as oxidative phosphorylation inhibitors, means that more clinical studies are needed to confirm the clinical utility of our findings.

A limitation of our study is that we did not obtain SALL4A- and SALL4B-specific hits. Further studies are needed to determine the unique mechanisms by which each isoform drives cancer. A confounding issue is that SALL4A and B are co-expressed from the same gene locus as splice isoforms, and from prior work, are always co-expressed in the same cell line or tumor tissue. Our study demonstrates that both SALL4 isoforms can functionally upregulate, and thus create a dependency on, oxidative phosphorylation. Targeting this pathway shared by both isoforms with oxidative phosphorylation inhibitors is therefore a viable therapeutic option for SALL4-expressing cancers. We have observed that SALL4 is upregulated in about 20-30% of all solid tumors[12,14], so the potential clinical utility of oxidative phosphorylation inhibitors with a companion SALL4 diagnostic is highly significant.

Our study demonstrates that a SALL4 biomarker can be used in conjunction with oligomycin, a highly potent oxidative phosphorylation inhibitor that has not yet been tested extensively in clinical trials to our knowledge. The LD33 (lethal dose that kills 33%) of oligomycin in rats is 0.5 mg/kg (1 mg/kg in mice), while 100% of rats survived with 0.1 mg/kg of drug (0.2 mg/kg in

mice)[28,48]. Our study doses mice at the sub-lethal dose of 0.1 mg/kg oligomycin, which is 10 times less than the LD33, and we observe significant and selective tumor size suppression in SALL4-high tumors with low toxicity. It might be worthwhile to explore the clinical use of oligomycin in SALL4-expressing tumors.

Figures Legends:

Fig. 1. A chemical genetic cell-based screen to identify compounds targeting SALL4 dependencies. (**A**) Schematic of screen involving the use of endogenous SALL4^{lo} and SALL4^{hi} HCC lines and engineered isogenic SALL4 expressing lines. (**B**) Venn diagram illustrating overlap of hit compounds which selectively decrease cell viability of the SALL4^{hi} lines over their respective SALL4^{lo} controls. (**C**) Workflow of natural product extract screen to identify individual compound hits from extracts containing multiple chemical entities.

Fig. 2. SALL4-dependent cells are susceptible to mitochondrial oxidative phosphorylation inhibitors. (**A**) Cell viability dose-response curves for cells treated for 96 hrs with hit compounds from the natural product extract screen, oligomycin, efrapeptin, antimycin, and leucinostatin, measured with CellTiter-Glo reagent and normalized to untreated cell viability (mean of 3 replicates ± SD). (**B**) Diagram indicating oxidative phosphorylation targets of validated hit compounds.

Fig. 3. Oligomycin A suppresses SALL4-dependent HCC. (**A**) Cell viability dose-response curves for a panel of HCC cell lines treated with oligomycin A for 72 hrs, measured with CellTiter-Glo reagent and normalized to untreated cell viability (mean of 3 replicates ± SD). (**B**) Tumor size plot of SALL4-high SNU-398 mouse xenografts injected (intraperitoneal) with vehicle, sorafenib, or oligomycin A (mean ± SD). (**C**) Plot of tumor size at day 13 of the xenograft experiments in (**B**) (mean ± SD). (**D**) Tumor size plot of SALL4-high PDX HCC26.1 mouse xenografts injected (intraperitoneal) with vehicle, sorafenib, oligomycin A, or a combination of 20 mg/kg sorafenib and 0.1 mg/kg oligomycin (mean ± SD). (**E**) Plot of tumor size at day 25 of the xenograft experiments in (**D**) (mean ± SD). (**F**) Tumor size plot of SALL4-low PDX1 mouse xenografts injected (intraperitoneal) with vehicle or oligomycin A (mean ± SD). (**G**) Plot of tumor size at day 32 of the xenograft experiments in (**F**) (mean ± SD). (**H-J**) Mouse weight quantification plot from the respective mouse xenograft experiments in (**B-G**) (mean ± SD).

Fig. 4. SALL4 binds and upregulates oxidative phosphorylation gene expression (**A**) Venn diagram of mitochondrial genes from the MitoCarta 2.0 dataset bound by SALL4 from our prior SALL4 ChIP-seq experiment performed on SNU-398 cells. Selected significant pathways from Gene Ontology analysis of the SALL4 bound genes are shown. (**B**) ChIP-seq region plots of the SALL4 bound mitochondrial genes in (**A**), representing the regions bound by SALL4 and marked by H3K27ac in SNU-398 cells (from analysis of prior data), −3 kb upstream of the transcription start site (TSS) and +3 kb downstream of the transcription end site (TES). (**C**) Representative ChIP-seq input, H3K27ac, and SALL4 peaks for control gene *SUMO1* and electron transport chain genes *ATP5D*, *ATP5E,* and *NDUFA3*. (**D**) RNA-seq expression level fold change for a panel of mitochondrial genes from the SALL4 bound list in (**A**), in the SALL4 expressing cell lines, normalized to expression levels in the empty vector control, performed in singlet. (**E**) Western blots for SALL4-bound oxidative phosphorylation genes and ACTB loading

control in the cell lines used in the screen. Bands were quantified by densitometry with SNU-387 and EV bands as references. (**F**) Western blots for the genes in (**E**) with *SALL4* knockdown for 72 hrs in the SNU-398 cell line. Bands were quantified by densitometry with sh-scr bands as reference.

Fig. 5. SALL4 expression upregulates oxidative phosphorylation (**A**) OCR measurements of SALL4 endogenous and isogenic lines used in the screen, normalized to DNA content measured by CyQUANT reagent (mean of 3 replicates ± SD). (**B**) OCR measurements for *SALL4* knockdown in SNU-398 endogenous SALL4-high cells, normalized to DNA content measured by CyQUANT reagent (mean of 3 replicates ± SD). (**C**) Representative images of SALL4 endogenous and isogenic cell lines stained with DAPI nuclear dye, Mitotracker Red mitochondrial membrane potential dye, and immunostained with cytochrome c antibody. Scale bars are 20 μm in length. (**D**) Quantification of cytochrome c fluorescence signal per cell, normalized to DAPI signal (median, quartile and range). (**E**) Quantification of MitoTracker fluorescence signal per cell, normalized to DAPI signal (median, quartile and range). (**F**) ATP levels per DNA content for the SALL4 isogenic cell lines measured by CellTiter-Glo ATP detection reagent values normalized to CyQUANT DNA quantification reagent values (mean of 3 replicates ± SD). (**G**) NADH/NAD+ values measured by HPLC-mass spectrometry metabolite profiling of the SALL4 isogenic cell lines (mean of 3 replicates ± SD).

References and Notes:

1. Patel MN, Halling-Brown MD, Tym JE, et al. Objective assessment of cancer genes for drug discovery. Nat Rev Drug Discov 2013;12:35–50.

2. Zheng W, Thorne N, McKew JC. Phenotypic screens as a renewed approach for drug discovery. Drug Discov Today 2013;18:1067–1073.

3. Wilding JL, Bodmer WF. Cancer cell lines for drug discovery and development. Cancer Res 2014;74:2377–2384.

4. Janzen WP. Screening Technologies for Small Molecule Discovery: The State of the Art. Chem Biol 2014;21:1162–1170.

5. Ferlay J, Soerjomataram I, Dikshit R, et al. Cancer incidence and mortality worldwide: sources, methods and major patterns in GLOBOCAN 2012. Int J Cancer J Int Cancer 2015;136:E359-386.

6. Bruix J, Raoul J-L, Sherman M, et al. Efficacy and safety of sorafenib in patients with advanced hepatocellular carcinoma: subanalyses of a phase III trial. J Hepatol 2012;57:821–829.

7. Bruix J, Qin S, Merle P, et al. Regorafenib for patients with hepatocellular carcinoma who progressed on sorafenib treatment (RESORCE): a randomised, double-blind, placebo-controlled, phase 3 trial. The Lancet 2017;389:56–66.

8. Celis JF de, Barrio R. Regulation and function of Spalt proteins during animal development. Int J Dev Biol 2009;53:1385–1398.

9. Tatetsu H, Kong NR, Chong G, et al. SALL4, the missing link between stem cells, development and cancer. Gene 2016.

10. **Zhang J**, **Tam W-L**, **Tong GQ**, et al. Sall4 modulates embryonic stem cell pluripotency and early embryonic development by the transcriptional regulation of Pou5f1. Nat Cell Biol 2006;8:1114–1123.

11. **Lim CY**, **Tam W-L**, **Zhang J**, et al. Sall4 Regulates Distinct Transcription Circuitries in Different Blastocyst-Derived Stem Cell Lineages. Cell Stem Cell 2008;3:543–554.

12. **Nicolè L**, **Sanavia T**, Veronese N, et al. Oncofetal gene SALL4 and prognosis in cancer: A systematic review with meta-analysis. Oncotarget 2017;8:22968–22979.

13. **Oikawa T**, **Kamiya A**, **Kakinuma S**, et al. Sall4 regulates cell fate decision in fetal hepatic stem/progenitor cells. Gastroenterology 2009;136:1000–1011.

14. Yong KJ, Gao C, Lim JSJ, et al. Oncofetal gene SALL4 in aggressive hepatocellular carcinoma. N Engl J Med 2013;368:2266–2276.

15. Rao S, Zhen S, Roumiantsev S, et al. Differential roles of Sall4 isoforms in embryonic stem cell pluripotency. Mol Cell Biol 2010;30:5364–5380.

16. Kohlhase J, Chitayat D, Kotzot D, et al. SALL4 mutations in Okihiro syndrome (Duane-radial ray syndrome), acro-renal-ocular syndrome, and related disorders. Hum Mutat 2005;26:176–183.

17. Elling U, Klasen C, Eisenberger T, et al. Murine inner cell mass-derived lineages depend on Sall4 function. Proc Natl Acad Sci U S A 2006;103:16319–16324.

18. Yang J, Gao C, Chai L, et al. A novel SALL4/OCT4 transcriptional feedback network for pluripotency of embryonic stem cells. PloS One 2010;5:e10766.

19. **Lu J**, **Jeong H-W**, Jeong H, et al. Stem cell factor SALL4 represses the transcriptions of PTEN and SALL1 through an epigenetic repressor complex. PloS One 2009;4:e5577.

20. Li A, Jiao Y, Yong KJ, et al. SALL4 is a new target in endometrial cancer. Oncogene 2015;34:63–72.

21. Li A, Yang Y, Gao C, et al. A SALL4/MLL/HOXA9 pathway in murine and human myeloid leukemogenesis. J Clin Invest 2013;123:4195–4207.

22. Ma Y, Cui W, Yang J, et al. SALL4, a novel oncogene, is constitutively expressed in human acute myeloid leukemia (AML) and induces AML in transgenic mice. Blood 2006;108:2726–2735.

23. Ng SB, Kanagasundaram Y, Fan H, et al. The 160K Natural Organism Library, a unique resource for natural products research. Nat Biotechnol 2018;36:570–573.

24. Slater EC. The mechanism of action of the respiratory inhibitor, antimycin. Biochim Biophys Acta BBA - Rev Bioenerg 1973;301:129–154.

25. Hong S, Pedersen PL. ATP Synthase and the Actions of Inhibitors Utilized To Study Its Roles in Human Health, Disease, and Other Scientific Areas. Microbiol Mol Biol Rev MMBR 2008;72:590–641.

26. Park S, Chapuis N, Bardet V, et al. PI-103, a dual inhibitor of Class IA phosphatidylinositide 3-kinase and mTOR, has antileukemic activity in AML. Leukemia 2008;22:1698–1706.

27. **Yong KJ**, **Li A**, **Ou W-B**, et al. Targeting SALL4 by entinostat in lung cancer. Oncotarget 2016;7:75425–75440.

28. Kramar R, Hohenegger M, Srour AN, et al. Oligomycin toxicity in intact rats. Agents Actions 1984;15:660–663.

29. Smith RM, Peterson WH, McCoy E. Oligomycin, a new antifungal antibiotic. Antibiot Chemother 1954;4:962-70.

30. Lu G-D, Ang YH, Zhou J, et al. CCAAT/enhancer binding protein α predicts poorer prognosis and prevents energy starvation–induced cell death in hepatocellular carcinoma. Hepatol Baltim Md 2015;61:965–978.

31. Holman R. Metformin as first choice in oral diabetes treatment: the UKPDS experience. Journ Annu Diabetol Hotel Dieu 2007:13–20.

32. Bridges HR, Jones AJY, Pollak MN, et al. Effects of metformin and other biguanides on oxidative phosphorylation in mitochondria. Biochem J 2014;462:475–487.

33. Fang M, Qu Y, Gao B, et al. Oligomycin, a Complex V Inhibitor, Decreases Left Ventricular Contractility in Isolated Rabbit Heart. FASEB J 2011;25:lb362–lb362.

34. **Liu BH**, **Jobichen C**, Chia CSB, et al. Targeting cancer addiction for SALL4 by shifting its transcriptome with a pharmacologic peptide. Proc Natl Acad Sci U S A 2018;115:E7119–E7128.

35. **Wang Z**, **Zang C**, **Rosenfeld JA**, et al. Combinatorial patterns of histone acetylations and methylations in the human genome. Nat Genet 2008;40:897–903.

36. **Subramanian A**, **Tamayo P**, Mootha VK, et al. Gene set enrichment analysis: a knowledge-based approach for interpreting genome-wide expression profiles. Proc Natl Acad Sci U S A 2005;102:15545–15550.

37. Xia J, Wishart DS. MSEA: a web-based tool to identify biologically meaningful patterns in quantitative metabolomic data. Nucleic Acids Res 2010;38:W71-77.

38. Lu M, Zhou L, Stanley WC, et al. Role of the Malate-Aspartate Shuttle on the Metabolic Response to Myocardial Ischemia. J Theor Biol 2008;254:466–475.

39. Courtnay R, Ngo DC, Malik N, et al. Cancer metabolism and the Warburg effect: the role of HIF-1 and PI3K. Mol Biol Rep 2015;42:841–851.

40. Phillips NR, Sprouse ML, Roby RK. Simultaneous quantification of mitochondrial DNA copy number and deletion ratio: A multiplex real-time PCR assay. Sci Rep 2014;4:3887.

41. Mendham AE, Duffield R, Coutts AJ, et al. Similar mitochondrial signaling responses to a single bout of continuous or small-sided-games-based exercise in sedentary men. J Appl Physiol Bethesda Md 1985 2016;121:1326–1334.

42. Eisele PS, Salatino S, Sobek J, et al. The peroxisome proliferator-activated receptor γ coactivator 1α/β (PGC-1) coactivators repress the transcriptional activity of NF-κB in skeletal muscle cells. J Biol Chem 2013;288:2246–2260.

43. LeBleu VS, O'Connell JT, Gonzalez Herrera KN, et al. PGC-1α mediates mitochondrial biogenesis and oxidative phosphorylation in cancer cells to promote metastasis. Nat Cell Biol 2014;16:992–1003, 1–15.

44. Vander Heiden MG, DeBerardinis RJ. Understanding the Intersections between Metabolism and Cancer Biology. Cell 2017;168:657–669.

45. DeBerardinis RJ, Chandel NS. Fundamentals of cancer metabolism. Sci Adv 2016;2:e1600200.

46. Palm W, Thompson CB. Nutrient acquisition strategies of mammalian cells. Nature 2017;546:234–242.

47. Ashton TM, McKenna WG, Kunz-Schughart LA, et al. Oxidative Phosphorylation as an Emerging Target in Cancer Therapy. Clin Cancer Res 2018;24:2482-90.

48. Freireich EJ, Gehan EA, Rall DP, et al. Quantitative comparison of toxicity of anticancer agents in mouse, rat, hamster, dog, monkey, and man. Cancer Chemother Rep 1966;50:219–244.

Author names in bold designate shared co-first authorship.

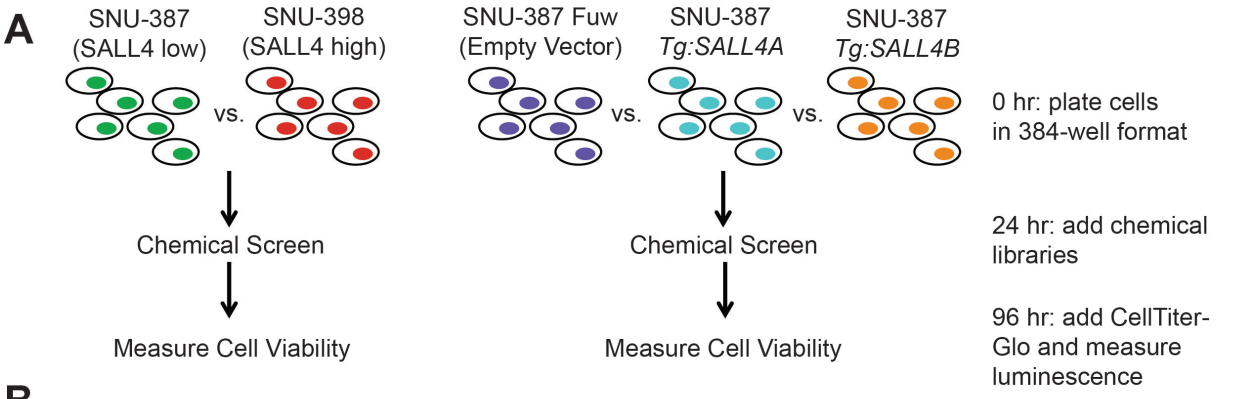
A
SNU-387
(SALL4 low)
vs.
SNU-398
(SALL4 high)
Chemical Screen
Measure Cell Viability
SNU-387 Fuw
(Empty Vector)
vs.
SNU-387
Tg:SALL4A
vs.
SNU-387
Tg:SALL4B
Chemical Screen
Measure Cell Viability
0 hr: plate cells in 384-well format
24 hr: add chemical libraries
96 hr: add CellTiter-Glo and measure luminescence

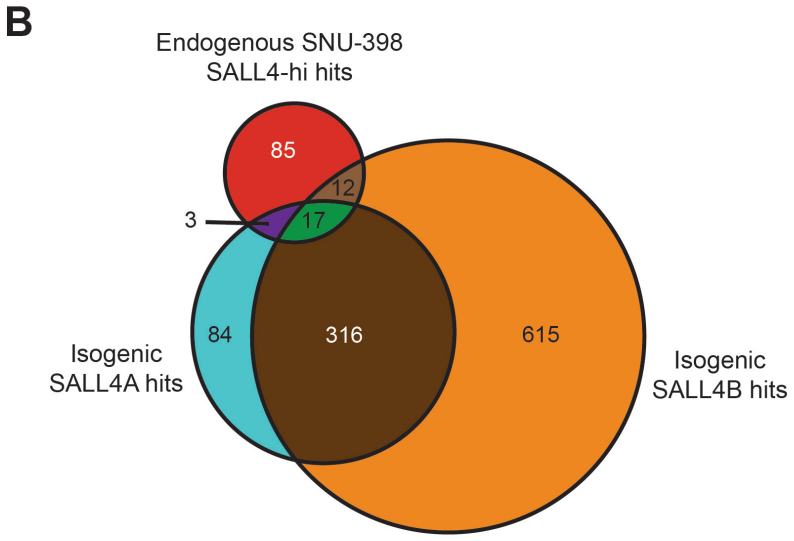
B
Endogenous SNU-398
SALL4-hi hits
85
12
3
17
84
316
615
Isogenic
SALL4A hits
Isogenic
SALL4B hits

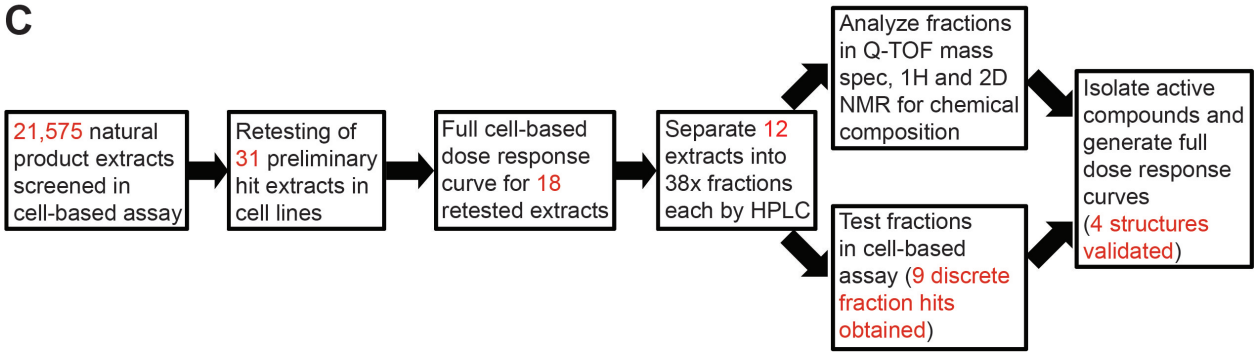
C
21,575 natural product extracts screened in cell-based assay
Retesting of 31 preliminary hit extracts in cell lines
Full cell-based dose response curve for 18 retested extracts
Separate 12 extracts into 38x fractions each by HPLC
Analyze fractions in Q-TOF mass spec, 1H and 2D NMR for chemical composition
Test fractions in cell-based assay (9 discrete fraction hits obtained)
Isolate active compounds and generate full dose response curves (4 structures validated)

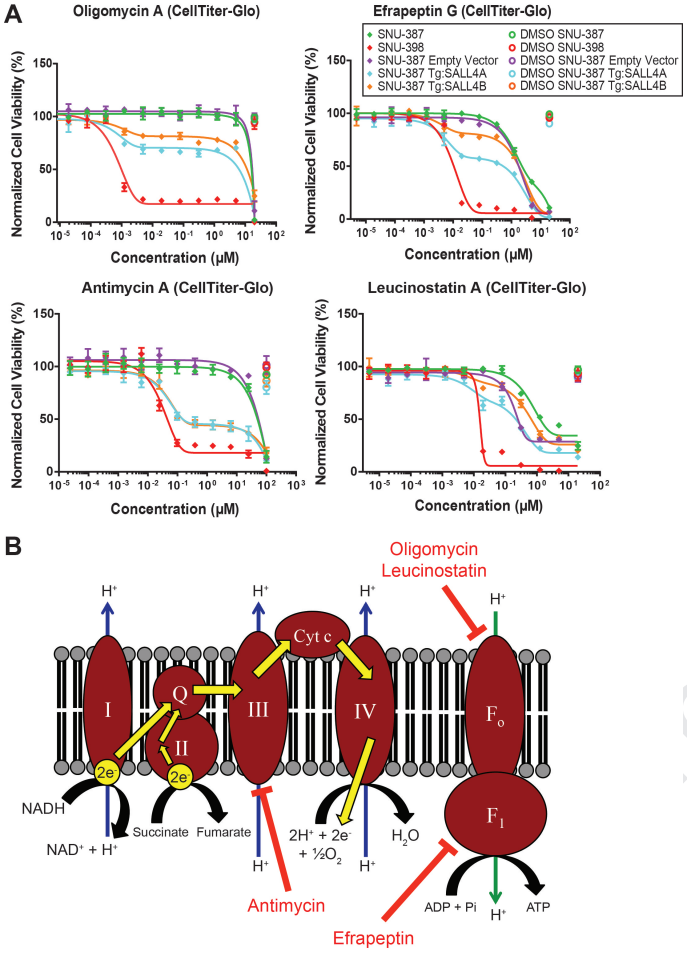
A
Oligomycin A (CellTiter-Glo)
Efrapeptin G (CellTiter-Glo)
Antimycin A (CellTiter-Glo)
Leucinostatin A (CellTiter-Glo)
Normalized Cell Viability (%)
Concentration (μM)
SNU-387
SNU-398
SNU-387 Empty Vector
SNU-387 Tg:SALL4A
SNU-387 Tg:SALL4B
DMSO SNU-387
DMSO SNU-398
DMSO SNU-387 Empty Vector
DMSO SNU-387 Tg:SALL4A
DMSO SNU-387 Tg:SALL4B

B
Oligomycin
Leucinostatin
H+
Cyt c
I
II
III
IV
Q
Fo
F1
2e-
NADH
NAD+ + H+
Succinate
Fumarate
2H+ + 2e- + ½O2
H2O
Antimycin
Efrapeptin
ADP + Pi
ATP

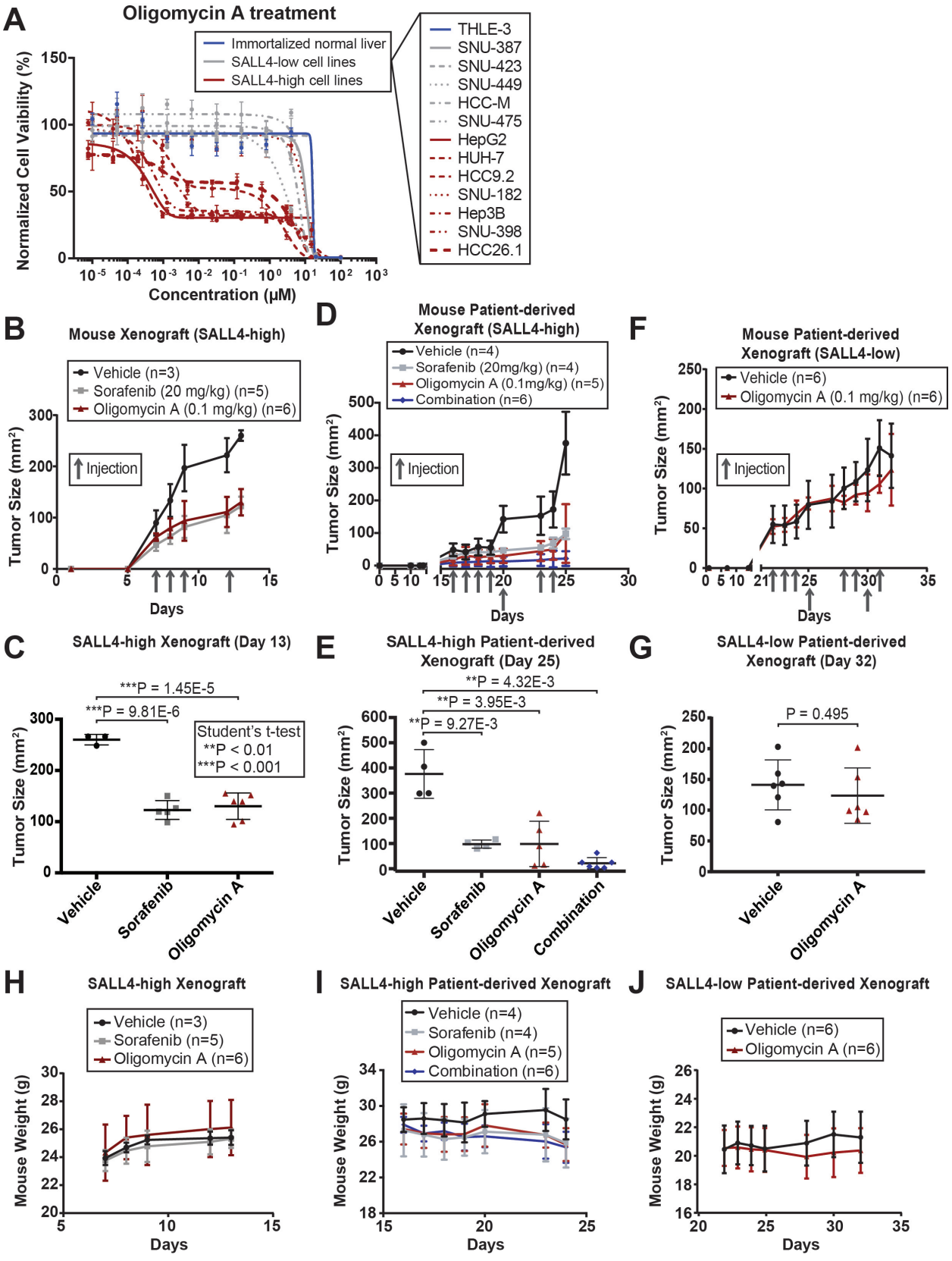
A
Oligomycin A treatment
Immortalized normal liver
SALL4-low cell lines
SALL4-high cell lines
THLE-3
SNU-387
SNU-423
SNU-449
HCC-M
SNU-475
HepG2
HUH-7
HCC9.2
SNU-182
Hep3B
SNU-398
HCC26.1
Normalized Cell Vaibility (%)
Concentration (μM)
B
Mouse Xenograft (SALL4-high)
Vehicle (n=3)
Sorafenib (20 mg/kg) (n=5)
Oligomycin A (0.1 mg/kg) (n=6)
Injection
Tumor Size (mm²)
Days
D
Mouse Patient-derived Xenograft (SALL4-high)
Vehicle (n=4)
Sorafenib (20mg/kg) (n=4)
Oligomycin A (0.1mg/kg) (n=5)
Combination (n=6)
Injection
Tumor Size (mm²)
Days
F
Mouse Patient-derived Xenograft (SALL4-low)
Vehicle (n=6)
Oligomycin A (0.1 mg/kg) (n=6)
Injection
Tumor Size (mm²)
Days
C
SALL4-high Xenograft (Day 13)
***P = 1.45E-5
***P = 9.81E-6
Student's t-test
**P < 0.01
***P < 0.001
Tumor Size (mm²)
Vehicle
Sorafenib
Oligomycin A
E
SALL4-high Patient-derived Xenograft (Day 25)
**P = 4.32E-3
**P = 3.95E-3
**P = 9.27E-3
Tumor Size (mm²)
Vehicle
Sorafenib
Oligomycin A
Combination
G
SALL4-low Patient-derived Xenograft (Day 32)
P = 0.495
Tumor Size (mm²)
Vehicle
Oligomycin A
H
SALL4-high Xenograft
Vehicle (n=3)
Sorafenib (n=5)
Oligomycin A (n=6)
Mouse Weight (g)
Days
I
SALL4-high Patient-derived Xenograft
Vehicle (n=4)
Sorafenib (n=4)
Oligomycin A (n=5)
Combination (n=6)
Mouse Weight (g)
Days
J
SALL4-low Patient-derived Xenograft
Vehicle (n=6)
Oligomycin A (n=6)
Mouse Weight (g)
Days

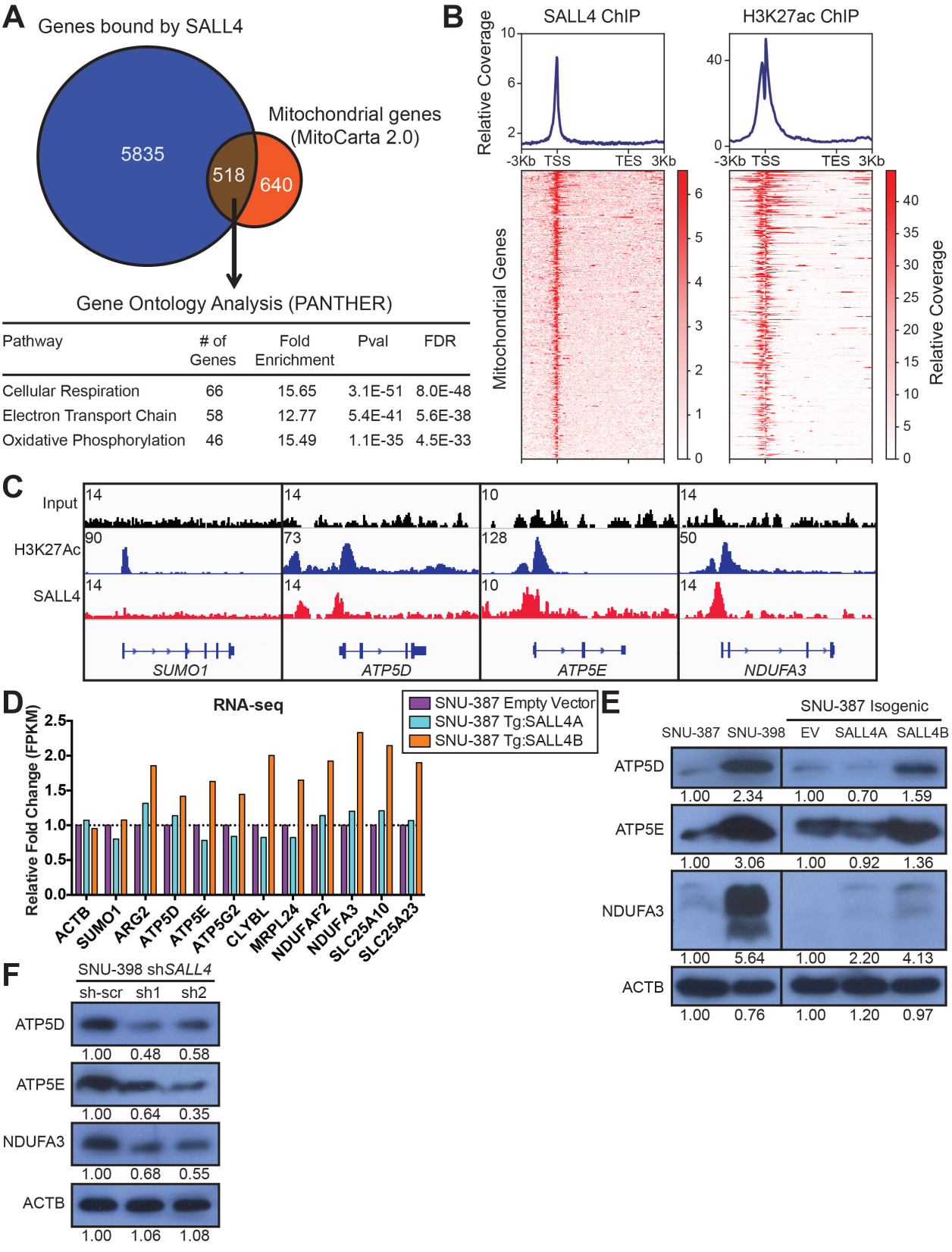

Pathway	# of Genes	Fold Enrichment	Pval	FDR
Cellular Respiration	66	15.65	3.1E-51	8.0E-48
Electron Transport Chain	58	12.77	5.4E-41	5.6E-38
Oxidative Phosphorylation	46	15.49	1.1E-35	4.5E-33

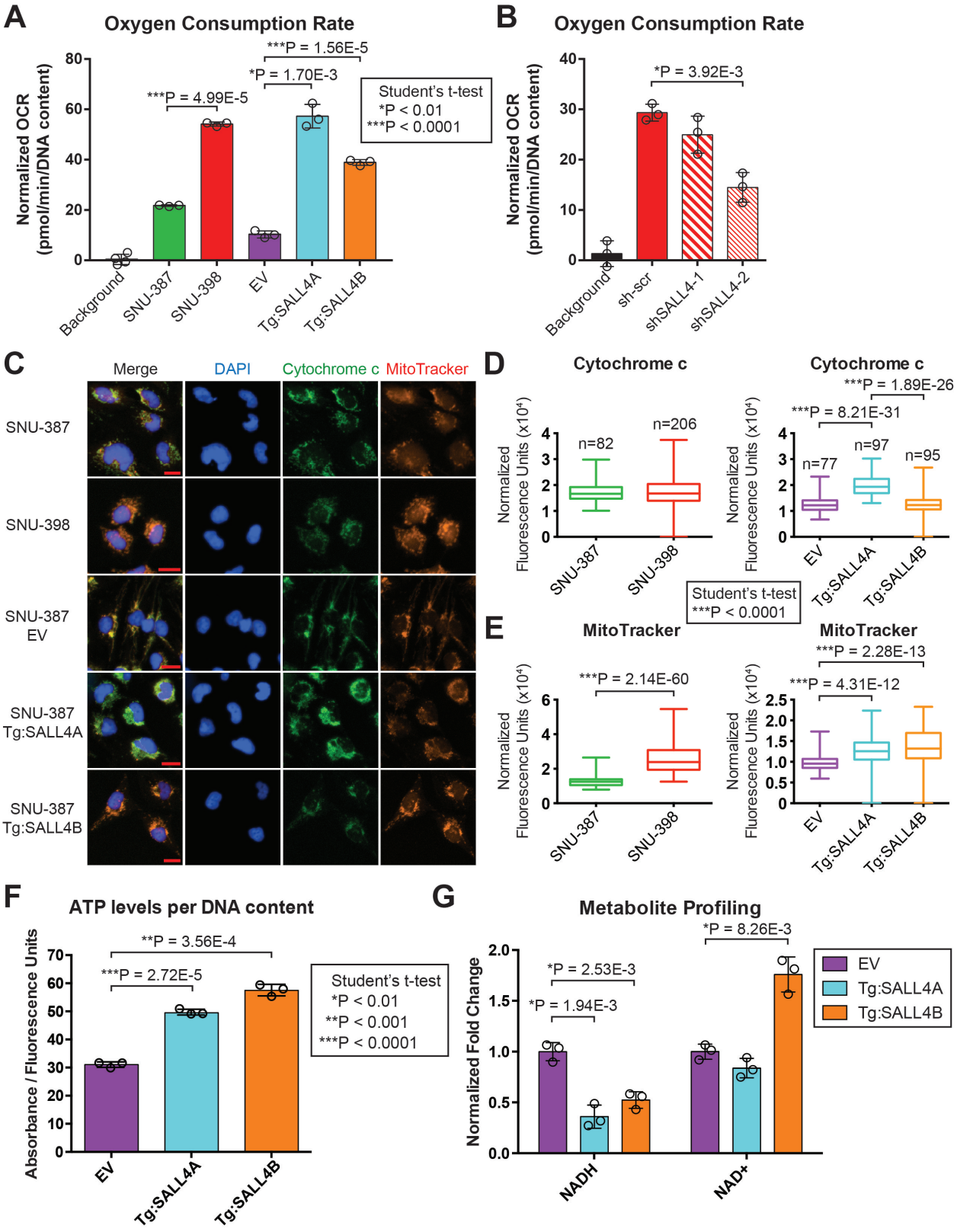
A
Oxygen Consumption Rate
Normalized OCR (pmol/min/DNA content)
***P = 1.56E-5
*P = 1.70E-3
***P = 4.99E-5
Student's t-test
*P < 0.01
***P < 0.0001
Background
SNU-387
SNU-398
EV
Tg:SALL4A
Tg:SALL4B
B
Oxygen Consumption Rate
Normalized OCR (pmol/min/DNA content)
*P = 3.92E-3
Background
sh-scr
shSALL4-1
shSALL4-2
C
Merge
DAPI
Cytochrome c
MitoTracker
SNU-387
SNU-398
SNU-387 EV
SNU-387 Tg:SALL4A
SNU-387 Tg:SALL4B
D
Cytochrome c
Normalized Fluorescence Units (x10⁴)
n=82
n=206
SNU-387
SNU-398
Cytochrome c
***P = 1.89E-26
***P = 8.21E-31
n=77
n=97
n=95
EV
Tg:SALL4A
Tg:SALL4B
Student's t-test
***P < 0.0001
E
MitoTracker
***P = 2.14E-60
MitoTracker
***P = 2.28E-13
***P = 4.31E-12
F
ATP levels per DNA content
Absorbance / Fluorescence Units
**P = 3.56E-4
***P = 2.72E-5
Student's t-test
*P < 0.01
**P < 0.001
***P < 0.0001
EV
Tg:SALL4A
Tg:SALL4B
G
Metabolite Profiling
Normalized Fold Change
*P = 8.26E-3
*P = 2.53E-3
*P = 1.94E-3
EV
Tg:SALL4A
Tg:SALL4B
NADH
NAD+

What you need to know:

BACKGROUND AND CONTEXT: The transcription factor SALL4 is mis-expressed in cancer cells. We developed a screen to identify compounds that reduce the viability of liver cancer cells that mis-express SALL4 and the mechanisms by which these compounds act.

NEW FINDINGS: We identified a metabolic vulnerability in liver (and possibly lung) cancer cells, due to overexpression of SALL4, which can be targeted by natural product oxidative phosphorylation inhibitors.

LIMITATIONS: This was a chemical screen for compounds that affect the viability of a small number of cell lines in culture and growth as xenograft tumors in mice. Additional studies in other animal models of liver cancer, and on other cell lines, are needed.

IMPACT: We developed a screen to identify compounds that kill cancer cells that overexpress or underexpress a specific protein. This screen can be used to identify compounds with toxicity to cells with other alterations in gene expression and identify the mechanisms regulated by these alterations.

Lay Summary: Liver tumors overexpress a protein called SALL4, which causes them to become dependent on specific metabolic pathways for survival. We identified a set of compounds that induce the death of these cancer cells by inhibiting this pathway.

Drug	SNU-387 (SALL4 low) IC50 (μM)	SNU-398 (SALL4 high) IC50 (μM)	Selectivity (low IC50 / high IC50)
PI-103	18	1.4	13
Oigomycin A	10	0.0005	20000
Oligomycin A, B and C mix	20	0.00098	20408
21-hydroxyoligomycin A	20	0.0076	2632
Efrapeptin D	11	0.015	733
Efrapeptin Eα	2	0.0051	392
Efrapeptin G	2	0.0092	217
Efrapeptin H	2	0.006	333
Antimycin A	50	0.004	12500
Leucinostatin A	1	0.002	500

Drug	SNU-387 (SALL4 low) IC50 (μM)	SNU-398 (SALL4 high) IC50 (μM)	Selectivity (low IC50 / high IC50)
Oigomycin A	7.5	0.001	7500

Symbol	Description
ABCA9	ATP-binding cassette, sub-family A (ABC1), member 9
ABCB10	ATP-binding cassette, sub-family B (MDR/TAP), member 10
ABCB6	ATP-binding cassette, sub-family B (MDR/TAP), member 6
ABCB8	ATP-binding cassette, sub-family B (MDR/TAP), member 8
ABCB9	ATP-binding cassette, sub-family B (MDR/TAP), member 9
ABCD2	ATP-binding cassette, sub-family D (ALD), member 2
ABCD3	ATP-binding cassette, sub-family D (ALD), member 3
ABCF2	ATP-binding cassette, sub-family F (GCN20), member 2
ABHD10	abhydrolase domain containing 10
ABHD11	abhydrolase domain containing 11
ACAA1	acetyl-CoA acyltransferase 1
ACACA	acetyl-CoA carboxylase alpha
ACACB	acetyl-CoA carboxylase beta
ACAD9	acyl-CoA dehydrogenase family, member 9
ACADM	acyl-CoA dehydrogenase, C-4 to C-12 straight chain
ACADVL	acyl-CoA dehydrogenase, very long chain
ACCS	1-aminocyclopropane-1-carboxylate synthase homolog (Arabidopsis)(non-functional)
ACLY	ATP citrate lyase
ACO1	aconitase 1, soluble
ACO2	aconitase 2, mitochondrial
ACOT7	acyl-CoA thioesterase 7
ACOX3	acyl-CoA oxidase 3, pristanoyl
ACP6	acid phosphatase 6, lysophosphatidic
ACYP2	acylphosphatase 2, muscle type
ADCK1	aarF domain containing kinase 1
ADCK3	aarF domain containing kinase 3
ADCK4	aarF domain containing kinase 4
ADCK5	aarF domain containing kinase 5
AFG3L2	AFG3-like AAA ATPase 2
AK2	adenylate kinase 2
AKAP1	A kinase (PRKA) anchor protein 1
AKAP10	A kinase (PRKA) anchor protein 10
AKR7A2	aldo-keto reductase family 7, member A2 (aflatoxin aldehyde reductase)
ALAS1	aminolevulinate, delta-, synthase 1
ALDH3A2	aldehyde dehydrogenase 3 family, member A2
ALKBH3	alkB, alkylation repair homolog 3 (E. coli)
AMACR	alpha-methylacyl-CoA racemase
ANGEL2	angel homolog 2 (Drosophila)
APOPT1	apoptogenic 1, mitochondrial
ARG2	arginase 2
ASAH2	N-acylsphingosine amidohydrolase (non-lysosomal ceramidase) 2
ATAD3A	ATPase family, AAA domain containing 3A
ATAD3B	ATPase family, AAA domain containing 3B
ATIC	5-aminoimidazole-4-carboxamide ribonucleotide formyltransferase/IMP cyclohydrolase
ATP5D	ATP synthase, H+ transporting, mitochondrial F1 complex, delta subunit
ATP5E	ATP synthase, H+ transporting, mitochondrial F1 complex, epsilon subunit
ATP5G1	ATP synthase, H+ transporting, mitochondrial Fo complex, subunit C1 (subunit 9)
ATP5G2	ATP synthase, H+ transporting, mitochondrial Fo complex, subunit C2 (subunit 9)
ATP5I	ATP synthase, H+ transporting, mitochondrial Fo complex, subunit E
ATP5O	ATP synthase, H+ transporting, mitochondrial F1 complex, O subunit
ATP5S	ATP synthase, H+ transporting, mitochondrial Fo complex, subunit s (factor B)
ATP5SL	ATP5S-like
ATXN2	ataxin 2
AUH	AU RNA binding protein/enoyl-CoA hydratase
AURKAIP1	aurora kinase A interacting protein 1

Rank	Gene Set	Gene count	Enrichment score	Normalized enrichment score	Nominal p-val	FDR q-val	FWER p-val	RANK AT MAX	LEADING EDGE
1	HALLMARK_MYC_TARGETS_V1	196	0.54422325	2.903786	<0.001	<0.001	<0.001	3117	tags=57%, list=24%, signal=74%
2	HALLMARK_E2F_TARGETS	196	0.45119676	2.416688	<0.001	<0.001	<0.001	3489	tags=48%, list=27%, signal=65%
3	HALLMARK_G2M_CHECKPOINT	191	0.4186637	2.1925008	<0.001	<0.001	<0.001	3592	tags=45%, list=28%, signal=61%
4	HALLMARK_OXIDATIVE_PHOSPHORYLATION	193	0.3870408	2.0754309	<0.001	0.0004	0.001	4453	tags=56%, list=35%, signal=84%
5	HALLMARK_FATTY_ACID_METABOLISM	124	0.3794251	1.9089539	<0.001	0.00244659	0.009	2613	tags=34%, list=20%, signal=42%
6	HALLMARK_MYC_TARGETS_V2	58	0.44597328	1.9018548	<0.001	0.00203883	0.009	4511	tags=71%, list=35%, signal=108%
7	HALLMARK_PANCREAS_BETA_CELLS	20	0.5358952	1.7685649	0.007246377	0.00404024	0.021	3376	tags=70%, list=26%, signal=95%
8	HALLMARK_WNT_BETA_CATENIN_SIGNALING	39	0.40879318	1.6528691	0.015503876	0.01053979	0.06	3624	tags=49%, list=28%, signal=68%
9	HALLMARK_MTORC1_SIGNALING	189	0.2773534	1.4608389	<0.001	0.04107863	0.245	3593	tags=39%, list=28%, signal=53%
10	HALLMARK_MITOTIC_SPINDLE	193	0.2657652	1.4121544	0.008130081	0.05260091	0.329	3861	tags=39%, list=30%, signal=55%
11	HALLMARK_ANGIOGENESIS	22	0.4013473	1.3787901	0.0925	0.06191985	0.399	2586	tags=41%, list=20%, signal=51%
12	HALLMARK_PI3K_AKT_MTOR_SIGNALING	88	0.2899007	1.3589194	0.037383176	0.06560664	0.44	3874	tags=47%, list=30%, signal=66%
13	HALLMARK_DNA_REPAIR	137	0.26718286	1.3469937	0.021201413	0.06728908	0.477	4039	tags=42%, list=31%, signal=60%
14	HALLMARK_ANDROGEN_RESPONSE	88	0.29277417	1.3432475	0.043887146	0.06404232	0.487	2888	tags=35%, list=22%, signal=45%
15	HALLMARK_GLYCOLYSIS	165	0.23361187	1.2149675	0.086142324	0.16305687	0.848	3351	tags=35%, list=26%, signal=46%
16	HALLMARK_TGF_BETA_SIGNALING	53	0.2779019	1.1678144	0.17886178	0.21046484	0.923	3059	tags=36%, list=24%, signal=47%
17	HALLMARK_UNFOLDED_PROTEIN_RESPONSE	106	0.22229196	1.0556718	0.32413793	0.40546182	0.993	3592	tags=34%, list=28%, signal=47%
18	HALLMARK_ADIPOGENESIS	169	0.19637655	1.0165602	0.42205322	0.4795793	0.998	2625	tags=25%, list=20%, signal=32%
19	HALLMARK_HEME_METABOLISM	157	0.19404869	1.004472	0.4522059	0.4878528	0.999	3248	tags=29%, list=25%, signal=39%
20	HALLMARK_PROTEIN_SECRETION	92	0.20814914	0.9693294	0.509375	0.55203885	0.999	4174	tags=39%, list=32%, signal=57%
21	HALLMARK_PEROXISOME	91	0.17128518	0.80474705	0.8702065	0.8828335	1	2947	tags=24%, list=23%, signal=31%

Rank	Gene Set	Gene count	Enrichment score	Normalized enrichment score	Nominal p-val	FDR q-val	FWER p-val	RANK AT MAX	LEADING EDGE
1	HALLMARK_TNFA_SIGNALING_VIA_NFKB	156	-0.45459783	-2.0974655	<0.001	<0.001	<0.001	3441	tags=49%, list=27%, signal=66%
2	HALLMARK_KRAS_SIGNALING_DN	86	-0.4672904	-1.9812888	<0.001	<0.001	<0.001	2459	tags=41%, list=19%, signal=50%
3	HALLMARK_INTERFERON_GAMMA_RESPONSE	130	-0.41349	-1.8862952	<0.001	8.38E-04	0.003	3471	tags=44%, list=27%, signal=59%
4	HALLMARK_KRAS_SIGNALING_UP	122	-0.3830037	-1.703266	<0.001	0.0114271	0.053	3365	tags=45%, list=26%, signal=60%
5	HALLMARK_INTERFERON_ALPHA_RESPONSE	63	-0.39885956	-1.6034104	0.003100775	0.02396705	0.134	3431	tags=43%, list=27%, signal=58%
6	HALLMARK_APOPTOSIS	126	-0.3316926	-1.4844469	0.008595988	0.06410802	0.375	2589	tags=31%, list=20%, signal=38%
7	HALLMARK_INFLAMMATORY_RESPONSE	111	-0.33296204	-1.4842857	0.005813954	0.05494973	0.375	3889	tags=48%, list=30%, signal=68%
8	HALLMARK_HYPOXIA	161	-0.31716335	-1.4745462	0.008032128	0.05338081	0.405	3131	tags=35%, list=24%, signal=45%
9	HALLMARK_UV_RESPONSE_UP	137	-0.30827212	-1.404627	0.021067416	0.09326451	0.629	1773	tags=23%, list=14%, signal=27%
10	HALLMARK_P53_PATHWAY	171	-0.28917313	-1.3605517	0.029023746	0.12670156	0.789	1840	tags=22%, list=14%, signal=26%
11	HALLMARK_EPITHELIAL_MESENCHYMAL_TRANSITION	160	-0.26905727	-1.2489592	0.096045196	0.28560853	0.978	1625	tags=20%, list=13%, signal=23%
12	HALLMARK_MYOGENESIS	132	-0.27447602	-1.2466431	0.10787172	0.26622012	0.979	3013	tags=30%, list=23%, signal=39%
13	HALLMARK_COAGULATION	81	-0.2895137	-1.2150875	0.14837712	0.30610412	0.993	3487	tags=41%, list=27%, signal=55%
14	HALLMARK_IL6_JAK_STAT3_SIGNALING	50	-0.3073006	-1.1906862	0.18354431	0.33441827	0.998	743	tags=14%, list=6%, signal=15%
15	HALLMARK_COMPLEMENT	132	-0.25579098	-1.1527556	0.19648094	0.39766258	1	3676	tags=37%, list=28%, signal=51%
16	HALLMARK_IL2_STAT5_SIGNALING	141	-0.24269316	-1.1036245	0.26902175	0.497507	1	1747	tags=20%, list=14%, signal=23%
17	HALLMARK_ALLOGRAFT_REJECTION	108	-0.24634904	-1.0750725	0.3371266	0.5461092	1	3347	tags=36%, list=26%, signal=48%
18	HALLMARK_UV_RESPONSE_DN	133	-0.23273733	-1.0567168	0.3347339	0.5668574	1	2676	tags=25%, list=21%, signal=31%
19	HALLMARK_APICAL_JUNCTION	147	-0.2279322	-1.0511376	0.3619186	0.5523831	1	1597	tags=19%, list=12%, signal=21%
20	HALLMARK_ESTROGEN_RESPONSE_LATE	147	-0.2231084	-1.0323237	0.3916084	0.5742521	1	634	tags=12%, list=5%, signal=12%
21	HALLMARK_APICAL_SURFACE	33	-0.29412365	-1.0264652	0.43192488	0.561653	1	2000	tags=30%, list=15%, signal=36%
22	HALLMARK_HEDGEHOG_SIGNALING	28	-0.28716204	-0.96032095	0.5083612	0.7118046	1	2052	tags=29%, list=16%, signal=34%
23	HALLMARK_BILE_ACID_METABOLISM	74	-0.23093244	-0.9477847	0.5518248	0.7136509	1	3220	tags=30%, list=25%, signal=39%
24	HALLMARK_SPERMATOGENESIS	78	-0.21840073	-0.9144027	0.60932946	0.7703243	1	1359	tags=15%, list=11%, signal=17%
25	HALLMARK_ESTROGEN_RESPONSE_EARLY	163	-0.19200788	-0.8973891	0.6953456	0.7827583	1	2740	tags=23%, list=21%, signal=29%
26	HALLMARK_XENOBIOTIC_METABOLISM	137	-0.17221908	-0.77554655	0.9101124	0.99863005	1	3005	tags=24%, list=23%, signal=31%
27	HALLMARK_NOTCH_SIGNALING	31	-0.22198269	-0.76860005	0.81391585	0.97040075	1	2120	tags=19%, list=16%, signal=23%
28	HALLMARK_REACTIVE_OXIGEN_SPECIES_PATHWAY	41	-0.19056673	-0.704662	0.9122807	0.99662876	1	3036	tags=24%, list=24%, signal=32%
29	HALLMARK_CHOLESTEROL_HOMEOSTASIS	65	-0.16615808	-0.665276	0.9785276	0.98081714	1	3603	tags=29%, list=28%, signal=40%

Rank	Gene Set	Gene count	Enrichment score	Normalized enrichment score	Nominal p-val	FDR q-val	FWER p-val	RANK AT MAX	LEADING EDGE
1	HALLMARK_INTERFERON_ALPHA_RESPONSE	63	0.5913248	1.8732966	<0.001	0.00154545	0.002	2425	tags=48%, list=19%, signal=58%
2	HALLMARK_PANCREAS_BETA_CELLS	20	0.69303125	1.7767193	0.002923977	0.00310069	0.008	967	tags=40%, list=7%, signal=43%
3	HALLMARK_KRAS_SIGNALING_UP	122	0.52421314	1.7628177	<0.001	0.00308816	0.012	2242	tags=36%, list=17%, signal=43%
4	HALLMARK_COAGULATION	81	0.5259883	1.7234503	0.00232288	0.0040106	0.021	2295	tags=38%, list=18%, signal=46%
5	HALLMARK_EPITHELIAL_MESENCHYMAL_TRANSITION	160	0.493705	1.7112775	<0.001	0.0036885	0.024	2057	tags=39%, list=16%, signal=46%
6	HALLMARK_INTERFERON_GAMMA_RESPONSE	130	0.4974793	1.6995739	<0.001	0.00345738	0.027	2094	tags=35%, list=16%, signal=42%
7	HALLMARK_COMPLEMENT	132	0.4628288	1.5813584	<0.001	0.0182552	0.156	2184	tags=30%, list=17%, signal=36%
8	HALLMARK_BILE_ACID_METABOLISM	74	0.4773267	1.5218341	0.007058824	0.03358193	0.305	2559	tags=41%, list=20%, signal=50%
9	HALLMARK_PEROXISOME	91	0.44861767	1.4573961	0.019002376	0.06098207	0.517	2559	tags=33%, list=20%, signal=41%
10	HALLMARK_ALLOGRAFT_REJECTION	108	0.4314686	1.4534789	0.010112359	0.05795202	0.535	2407	tags=32%, list=19%, signal=40%
11	HALLMARK_APICAL_SURFACE	33	0.51475394	1.4487585	0.046791445	0.05516059	0.551	1145	tags=21%, list=9%, signal=23%
12	HALLMARK_INFLAMMATORY_RESPONSE	111	0.3878241	1.3112736	0.056647398	0.1887083	0.947	2209	tags=26%, list=17%, signal=31%
13	HALLMARK_HYPOXIA	161	0.36895123	1.2833416	0.07096774	0.2214807	0.977	3422	tags=41%, list=27%, signal=55%
14	HALLMARK_PROTEIN_SECRETION	92	0.39408895	1.2806478	0.08944954	0.20991223	0.977	3403	tags=36%, list=26%, signal=48%
15	HALLMARK_KRAS_SIGNALING_DN	86	0.38224345	1.2540939	0.116763	0.24408081	0.989	1567	tags=26%, list=12%, signal=29%
16	HALLMARK_MYOGENESIS	132	0.36284634	1.2478064	0.10843374	0.24098326	0.992	2602	tags=32%, list=20%, signal=39%
17	HALLMARK_ANGIOGENESIS	22	0.46687984	1.2221323	0.19971672	0.2746853	0.998	2356	tags=45%, list=18%, signal=56%
18	HALLMARK_SPERMATOGENESIS	78	0.3581901	1.144081	0.24214202	0.44036126	1	1452	tags=15%, list=11%, signal=17%
19	HALLMARK_APICAL_JUNCTION	147	0.3143143	1.0748835	0.34323433	0.6133307	1	2121	tags=22%, list=16%, signal=27%
20	HALLMARK_XENOBIOTIC_METABOLISM	137	0.30853093	1.06496	0.34323433	0.61134	1	3266	tags=31%, list=25%, signal=41%
21	HALLMARK_UV_RESPONSE_DN	133	0.30670384	1.0638742	0.34444445	0.584868	1	1591	tags=17%, list=12%, signal=19%
22	HALLMARK_IL6_JAK_STAT3_SIGNALING	50	0.33766794	1.0140747	0.46201745	0.70199645	1	2611	tags=32%, list=20%, signal=40%
23	HALLMARK_FATTY_ACID_METABOLISM	124	0.2884738	0.98608077	0.5106383	0.75306004	1	3871	tags=37%, list=30%, signal=52%
24	HALLMARK_GLYCOLYSIS	165	0.283843	0.9825379	0.52029914	0.73141646	1	3568	tags=35%, list=28%, signal=47%
25	HALLMARK_HEDGEHOG_SIGNALING	28	0.34655076	0.957465	0.5416667	0.76611716	1	1649	tags=25%, list=13%, signal=29%
26	HALLMARK_ADIPOGENESIS	169	0.26693162	0.93343526	0.6099366	0.7967666	1	3970	tags=38%, list=31%, signal=54%
27	HALLMARK_APOPTOSIS	126	0.27075914	0.9135117	0.6460369	0.8131792	1	2328	tags=22%, list=18%, signal=27%
28	HALLMARK_UV_RESPONSE_UP	137	0.2636504	0.90614545	0.67320263	0.80246556	1	1891	tags=16%, list=15%, signal=19%
29	HALLMARK_IL2_STAT5_SIGNALING	141	0.22654241	0.7804112	0.88273615	1	1	2403	tags=23%, list=19%, signal=28%
30	HALLMARK_TNFA_SIGNALING_VIA_NFKB	156	0.22286798	0.7703876	0.9001074	0.9887274	1	2229	tags=22%, list=17%, signal=26%
31	HALLMARK_CHOLESTEROL_HOMEOSTASIS	65	0.22961663	0.7263374	0.89205956	1	1	3975	tags=42%, list=31%, signal=60%
32	HALLMARK_OXIDATIVE_PHOSPHORYLATION	193	0.17608693	0.622198	0.9989362	1	1	4064	tags=37%, list=31%, signal=53%
33	HALLMARK_HEME_METABOLISM	157	0.16875547	0.5843203	0.9978425	1	1	3848	tags=35%, list=30%, signal=49%
34	HALLMARK_PI3K_AKT_MTOR_SIGNALING	88	0.15667826	0.5101099	1	0.9983632	1	1741	tags=8%, list=13%, signal=9%

Rank	Gene Set	Gene count	Enrichment score	Normalized enrichment score	Nominal p-val	FDR q-val	FWER p-val	RANK AT MAX	LEADING EDGE
1	HALLMARK_G2M_CHECKPOINT	191	-0.58563834	-2.7534144	<0.001	<0.001	<0.001	3952	tags=67%, list=31%, signal=95%
2	HALLMARK_E2F_TARGETS	196	-0.585082	-2.7252078	<0.001	<0.001	<0.001	3460	tags=62%, list=27%, signal=83%
3	HALLMARK_MYC_TARGETS_V2	58	-0.6770428	-2.6333227	<0.001	<0.001	<0.001	3128	tags=74%, list=24%, signal=97%
4	HALLMARK_MYC_TARGETS_V1	196	-0.5417159	-2.5153508	<0.001	<0.001	<0.001	4154	tags=63%, list=32%, signal=91%
5	HALLMARK_WNT_BETA_CATENIN_SIGNALING	39	-0.3811033	-1.355342	0.07053942	0.11256133	0.205	1219	tags=26%, list=9%, signal=28%
6	HALLMARK_UNFOLDED_PROTEIN_RESPONSE	106	-0.3134459	-1.3490728	0.010309278	0.09792489	0.211	3237	tags=37%, list=25%, signal=49%
7	HALLMARK_MITOTIC_SPINDLE	193	-0.28740817	-1.3351529	<0.001	0.09336001	0.234	3523	tags=35%, list=27%, signal=48%
8	HALLMARK_DNA_REPAIR	137	-0.2824273	-1.2578512	0.056818184	0.15466166	0.394	3076	tags=31%, list=24%, signal=41%
9	HALLMARK_ESTROGEN_RESPONSE_EARLY	163	-0.2661386	-1.2108046	0.028169014	0.2003904	0.519	1614	tags=25%, list=13%, signal=28%
10	HALLMARK_ESTROGEN_RESPONSE_LATE	147	-0.26500106	-1.1992086	0.07954545	0.19261722	0.545	2414	tags=32%, list=19%, signal=39%
11	HALLMARK_ANDROGEN_RESPONSE	88	-0.2664247	-1.1377987	0.15873016	0.27821615	0.718	1582	tags=18%, list=12%, signal=21%
12	HALLMARK_TGF_BETA_SIGNALING	53	-0.28065097	-1.0586255	0.34343433	0.4225494	0.882	1236	tags=13%, list=10%, signal=15%
13	HALLMARK_MTORC1_SIGNALING	189	-0.21982376	-1.0321668	0.45238096	0.46162638	0.918	3351	tags=29%, list=26%, signal=39%
14	HALLMARK_REACTIVE_OXIGEN_SPECIES_PATHWAY	41	-0.2472416	-0.89039975	0.6814159	0.8461123	0.995	2605	tags=27%, list=20%, signal=34%
15	HALLMARK_NOTCH_SIGNALING	31	-0.25944173	-0.8851398	0.7035573	0.80249673	0.995	727	tags=13%, list=6%, signal=14%
16	HALLMARK_P53_PATHWAY	171	-0.18341176	-0.8738643	0.89705884	0.7768563	0.995	1539	tags=13%, list=12%, signal=15%

Rank	Gene Set	Gene count	Enrichment score	Normalized enrichment score	Nominal p-val	FDR q-val	FWER p-val	RANK AT MAX	LEADING EDGE
1	HALLMARK_EPITHELIAL_MESENCHYMAL_TRANSITION	160	0.5631628	1.8430233	<0.001	7.08E-04	0.001	1931	tags=43%, list=15%, signal=50%
2	HALLMARK_KRAS_SIGNALING_UP	122	0.546754	1.7617139	<0.001	0.00292092	0.008	1523	tags=34%, list=12%, signal=39%
3	HALLMARK_PANCREAS_BETA_CELLS	20	0.6420886	1.606871	0.017402945	0.02228971	0.088	1805	tags=50%, list=14%, signal=58%
4	HALLMARK_APICAL_SURFACE	33	0.5892531	1.6029812	0.010256411	0.0174725	0.092	1513	tags=33%, list=12%, signal=38%
5	HALLMARK_COAGULATION	81	0.51908475	1.5955353	<0.001	0.0147415	0.097	2435	tags=42%, list=19%, signal=51%
6	HALLMARK_INTERFERON_GAMMA_RESPONSE	130	0.46743816	1.514262	0.003161222	0.0349614	0.25	2785	tags=41%, list=22%, signal=51%
7	HALLMARK_APICAL_JUNCTION	147	0.44177133	1.4351584	0.007329843	0.07794385	0.514	2224	tags=31%, list=17%, signal=37%
8	HALLMARK_INFLAMMATORY_RESPONSE	111	0.44543543	1.4149647	0.014721346	0.08471427	0.592	2026	tags=33%, list=16%, signal=39%
9	HALLMARK_UV_RESPONSE_DN	133	0.42810997	1.384296	0.014830508	0.10675002	0.718	2104	tags=29%, list=16%, signal=34%
10	HALLMARK_COMPLEMENT	132	0.4239892	1.3654386	0.022269353	0.11735058	0.797	2210	tags=28%, list=17%, signal=33%
11	HALLMARK_SPERMATOGENESIS	78	0.43680698	1.3588853	0.0389755	0.11440013	0.823	1655	tags=21%, list=13%, signal=23%
12	HALLMARK_INTERFERON_ALPHA_RESPONSE	63	0.4066165	1.2137375	0.18764044	0.39996493	1	3243	tags=40%, list=25%, signal=53%
13	HALLMARK_KRAS_SIGNALING_DN	86	0.37158516	1.162296	0.2236842	0.53856945	1	1893	tags=31%, list=15%, signal=37%
14	HALLMARK_HEDGEHOG_SIGNALING	28	0.44328576	1.1480955	0.27212682	0.54965526	1	2072	tags=43%, list=16%, signal=51%
15	HALLMARK_TGF_BETA_SIGNALING	53	0.37623885	1.112709	0.31609872	0.6414548	1	3518	tags=43%, list=27%, signal=59%
16	HALLMARK_MYOGENESIS	132	0.3378262	1.0809702	0.3478261	0.72114754	1	2029	tags=24%, list=16%, signal=28%
17	HALLMARK_PEROXISOME	91	0.3442629	1.0642002	0.3785558	0.7400807	1	2064	tags=18%, list=16%, signal=21%
18	HALLMARK_IL2_STAT5_SIGNALING	141	0.32731044	1.0589854	0.38164756	0.7169069	1	2277	tags=28%, list=18%, signal=33%
19	HALLMARK_ALLOGRAFT_REJECTION	108	0.32650065	1.036036	0.41802388	0.755652	1	3366	tags=39%, list=26%, signal=52%
20	HALLMARK_PROTEIN_SECRETION	92	0.3327136	1.0340518	0.43964562	0.7247107	1	3670	tags=36%, list=28%, signal=50%
21	HALLMARK_ESTROGEN_RESPONSE_EARLY	163	0.31122908	1.0194298	0.45454547	0.7357337	1	1742	tags=20%, list=13%, signal=23%
22	HALLMARK_NOTCH_SIGNALING	31	0.36926675	0.9955963	0.5	0.7750277	1	1186	tags=19%, list=9%, signal=21%
23	HALLMARK_ANGIOGENESIS	22	0.39032885	0.9799597	0.5107239	0.78438073	1	1931	tags=41%, list=15%, signal=48%
24	HALLMARK_WNT_BETA_CATENIN_SIGNALING	39	0.32578796	0.9079758	0.61042184	0.94310534	1	914	tags=13%, list=7%, signal=14%
25	HALLMARK_TNFA_SIGNALING_VIA_NFKB	156	0.2672464	0.8707608	0.7606218	0.99170715	1	1896	tags=22%, list=15%, signal=26%
26	HALLMARK_PI3K_AKT_MTOR_SIGNALING	88	0.28026617	0.86962026	0.7155172	0.95581174	1	3821	tags=31%, list=30%, signal=43%
27	HALLMARK_HYPOXIA	161	0.2651018	0.858664	0.7832461	0.943692	1	2104	tags=21%, list=16%, signal=25%
28	HALLMARK_UV_RESPONSE_UP	137	0.24478073	0.7989102	0.86	1	1	1934	tags=15%, list=15%, signal=18%
29	HALLMARK_IL6_JAK_STAT3_SIGNALING	50	0.27176604	0.79383034	0.80595237	0.99103963	1	3954	tags=44%, list=31%, signal=63%
30	HALLMARK_XENOBIOTIC_METABOLISM	137	0.22142082	0.7099682	0.9447917	1	1	1524	tags=12%, list=12%, signal=14%
31	HALLMARK_HEME_METABOLISM	157	0.21620384	0.70383143	0.9590164	1	1	3457	tags=27%, list=27%, signal=36%
32	HALLMARK_ANDROGEN_RESPONSE	88	0.21335027	0.66356516	0.9627193	1	1	2334	tags=19%, list=18%, signal=23%
33	HALLMARK_BILE_ACID_METABOLISM	74	0.19959146	0.611472	0.9865471	1	1	2502	tags=19%, list=19%, signal=23%
34	HALLMARK_MITOTIC_SPINDLE	193	0.17491393	0.5790194	0.9979571	0.9925043	1	4116	tags=28%, list=32%, signal=41%

Rank	Gene Set	Gene count	Enrichment score	Normalized enrichment score	Nominal p-val	FDR q-val	FWER p-val	RANK AT MAX	LEADING EDGE
1	HALLMARK_MYC_TARGETS_V2	58	-0.56738687	-2.2106073	<0.001	<0.001	<0.001	3291	tags=55%, list=26%, signal=74%
2	HALLMARK_MYC_TARGETS_V1	196	-0.40018487	-1.8356504	<0.001	0.00532222	0.004	3314	tags=42%, list=26%, signal=55%
3	HALLMARK_OXIDATIVE_PHOSPHORYLATION	193	-0.3796833	-1.8051862	<0.001	0.00354815	0.004	3075	tags=35%, list=24%, signal=45%
4	HALLMARK_E2F_TARGETS	196	-0.35362375	-1.6505095	<0.001	0.02034265	0.024	4179	tags=44%, list=32%, signal=64%
5	HALLMARK_REACTIVE_OXIGEN_SPECIES_PATHWAY	41	-0.41578227	-1.5237955	0.016574586	0.03757852	0.05	2129	tags=34%, list=16%, signal=41%
6	HALLMARK_UNFOLDED_PROTEIN_RESPONSE	106	-0.34554195	-1.4913799	<0.001	0.03902749	0.062	3980	tags=44%, list=31%, signal=64%
7	HALLMARK_DNA_REPAIR	137	-0.30922142	-1.4292427	<0.001	0.05762914	0.099	3507	tags=42%, list=27%, signal=57%
8	HALLMARK_ESTROGEN_RESPONSE_LATE	147	-0.30134118	-1.3489654	0.029411765	0.08971082	0.167	1242	tags=22%, list=10%, signal=25%
9	HALLMARK_P53_PATHWAY	171	-0.28487146	-1.2902381	<0.001	0.11728057	0.238	867	tags=15%, list=7%, signal=15%
10	HALLMARK_APOPTOSIS	126	-0.23724325	-1.0542336	0.29090908	0.52755076	0.751	1367	tags=19%, list=11%, signal=21%
11	HALLMARK_MTORC1_SIGNALING	189	-0.22427857	-1.0487995	0.2631579	0.4988658	0.764	2557	tags=21%, list=20%, signal=25%
12	HALLMARK_CHOLESTEROL_HOMEOSTASIS	65	-0.24175626	-0.9705008	0.5221239	0.7094553	0.897	1348	tags=17%, list=10%, signal=19%
13	HALLMARK_GLYCOLYSIS	165	-0.195801	-0.9216001	0.78125	0.80518925	0.94	1689	tags=18%, list=13%, signal=20%
14	HALLMARK_FATTY_ACID_METABOLISM	124	-0.21238084	-0.92060536	0.76785713	0.7504106	0.942	3561	tags=35%, list=28%, signal=47%
15	HALLMARK_G2M_CHECKPOINT	191	-0.19583482	-0.91855943	0.8181818	0.7079213	0.944	4300	tags=39%, list=33%, signal=57%
16	HALLMARK_ADIPOGENESIS	169	-0.19029619	-0.8485383	0.92105263	0.81371844	0.97	3205	tags=30%, list=25%, signal=39%

Title: New High-throughput Screen Identifies Compounds That Reduce Viability Specifically In Liver Cancer Cells That Express High Levels of SALL4 by Inhibiting Oxidative Phosphorylation

Authors: Justin L. Tan[1,2], **Feng Li**[1], Joanna Z. Yeo[1,2], Kol Jia Yong[1], Mahmoud A. Bassal[1,3,], Guo Hao Ng[2], May Yin Lee[2], Chung Yan Leong[4], Hong Kee Tan[1], Chan-shuo Wu[1], Bee Hui Liu[1], Tim H. Chan[1], Zi Hui Tan[1], Yun Shen Chan[2], Siyu Wang[2], Zhi Han Lim[2], Tan Boon Toh[1], Lissa Hooi[1], Kia Ngee Low[4], Siming Ma[2], Nikki R. Kong[5], Alicia J. Stein[5], Yue Wu[5,6], Matan T. Thangavelu[2], Atsushi Suzuki[7], Giridharan Periyasamy[2], John M. Asara[8], Yock Young Dan[1,9,10], Glenn K. Bonney[11,12], Edward K. Chow[1,13], Guo-Dong Lu[1,14,15], Huck Hui Ng[2], Yoganathan Kanagasundaram[4], Siew Bee Ng[4], Wai Leong Tam[1,2,16,17†], Daniel G. Tenen[1,3,†] & Li Chai[5†].

Author names in bold designate shared co-first authorship.

[†]Equal contribution.

Supplemental Materials and Methods:

Antibodies

Western blot antibodies are ACTB from Cell Signaling Technology (4970S), ARG2 from Abcam (ab137069), ATP5D from Abcam (ab97491), ATP5E from Santa Cruz Biotechnology (sc-393695), ATP5G2 from Abcam (ab80325), CASP3 from Cell Signaling Technology (9662), Cleaved CASP3 from Cell Signaling Technology (9661S), MRPL24 from Santa Cruz Biotechnology (sc-393858), NDUFA3 from Abcam (ab68089), SALL4 from Santa Cruz Biotechnology (sc-101147), and SLC25A23 from Santa Cruz Biotechnology (sc-377109). The SALL4 antibody used for immunohistochemistry is from Santa Cruz Biotechnology (sc-101147). The antibody used for immunofluorescence is Cytochrome c from BD Biosciences (556432).

Cell culture

Human hepatocellular carcinoma cell lines SNU-387, SNU-398, SNU-182, SNU-423, SNU-475, SNU-449, and HCC-M, and non small cell lung cancer cell lines H1299 and H661 (ATCC) were grown on standard tissue culture plates in filter sterilized RPMI (Gibco) with 10% heat-inactivated Fetal Bovine Serum (HyClone), 2 mM L-Glutamine (Gibco), and 1% Penicillin-Streptomycin (Gibco). Human hepatocellular carcinoma cell lines HepG2, Hep3B, and Huh-7 (ATCC) are grown on standard tissue culture plates in filter sterilized DMEM (Gibco) with 10% heat-inactivated Fetal Bovine Serum (HyClone), 2 mM L-Glutamine (Gibco), and 1% Penicillin-Streptomycin (Gibco). Human immortalized liver cell line THLE-3 is grown on standard tissue culture plates in filtered BEGM with additives (Lonza), 10% heat-inactivated Fetal Bovine Serum (HyClone), and 1% Penicillin-Streptomycin (Gibco). Cells are incubated at 37°C in a humidified atmosphere of 5% CO_2. Primary HCC cell lines HCC9.2 and HCC26.1 are culture in a media containing Advanced F12/DMEM reduced serum medium (1:1) (Gibco. 12643), 10mM HEPEs (Gibco), 100U/ml Pen /Strep (Gibco), 2mM L-Glutamine (Gibco), 1% N2 (Gibco), 2% B27 (Gibco), 50ng/ml EGF (Millipore), 250ng/ml R-Spondin1 (R&D), and 2µM SB431542 (Tocris). The cells are cultured on standard tissue culture dish coated with 3% matrigel (corning). Cells are incubated at 37°C in a humidified atmosphere of 5% CO_2.

Natural product extract dereplication

Active extracts were subjected to a dereplication procedure as described in the literature[1]. Active fractions were analyzed by accurate MS and MS-MS, and data matched against accurate mass of natural product compounds and A*STAR containing accurate mass and MS/MS mass spectra records of compounds that have been analysed under the same conditions. Oligomycin, 21-hydroxy oligomycin A, leucinostatin A and antimycin A were dereplicated by this method[1].

Fungi Strain F36017 Fermentation (Efrapeptin producing)

F36017 *Tolypocladium niveum* is a soil fungus isolated from United Kingdom. A 7 day old culture of F36017 grown on malt extract agar (Oxoid) was used to prepare 5 flasks of seed cultures, comprising of 50mL of seed medium [yeast extract 4 g/L (BD), malt extract 10g/L (Sigma), glucose 4 g/L (1^{st} Base), pH 5.5] placed in 250 mL Erlenmeyer flasks. These Seed cultures were allowed to grow for 5 days at 24°C with shaking at 200 rpm. At the end of the incubation period, the 5 flasks of seed cultures were combined and homogenized using rotor stator homogenizer (Omni). 5mL of the homogenized seed culture were then used to inoculate each of the 40 flasks containing 6g of vermiculite and 50mL of fermentation medium [maltose 30g/L (Sigma), glucose 10 g/L (1^{st} Base), yeast extract 0.8 g/L (BD), peptone 2 g/L (Oxoid), potassium phosphate monobasic 0.5 g/L (Sigma), magnesium sulphate heptahydrate 0.5 g/L (Merck), ferric chloride 10 mg/L (Sigma), zinc sulphate 2 mg/L (Merck), calcium chloride 55 mg/L (Sigma), pH 6.0]. Static fermentation was carried out for 14 days at 24°C. At the end of the incubation period, the cultures from all 40 flasks were harvested and freeze dried. The dried vermiculite cakes in each flask were scrambled lightly before extracting overnight 2 times with 100 mL methanol per flask. The insoluble materials from each extraction were removed by passing the mixtures through cellulose filter paper (Whatman Grade 4), and the filtrates were dried by rotary evaporation.

Efrapeptin isolation

The culture broths (40× 50 mL, total 2 L) of *Tolypociadium niveum* (F36017 were combined and freeze-dried, partitioned with DCM:MeOH:H_2O 1:1:1. The organic layer was then evaporated to dryness using rotary evaporation. The dried dichloromethane crude extract (0.7 g) was re-dissolved in methanol and separated by C18 reversed-phase preparative HPLC (solvent A: H2O + 0.1% HCOOH, solvent B: ACN + 0.1% HCOOH; flow rate: 30 mL/min, gradient conditions: 70:30 isocratic for 3 minutes; 30% to 40% of solvent B over 12 minutes, 30% to 65% of solvent B over 60 minutes, followed by 65% to 100% of solvent B over 15 minutes, and finally isocratic at 100% of solvent B for 20 minutes) to give 0.6 mg of efrapeptin D (**1,** RT 18.5 min.), 1.0 mg of efrapeptin Eα (**2,** RT 20 min.), 0.5 mg of efrapeptin G (**3,** RT 25min.), and 1.0 mg of efrapeptin H (**4,** RT 27 min.). Efrapeptins were elucidated by comparison accurate mass and ^{1}H NMR data to those of efrapeptins published with activity against bacteria and tumour cells[2].

Drug treatment

Drugs used in the study are PI-103 (Selleckchem), oligomycin A (Selleckchem, LKT Labs), 21-hydroxy oligomycin A (Enzo Life Sciences), oligomycin A, B, and C mix (Enzo Life Sciences), sorafenib tosylate (Selleckchem), bortezomib (Selleckchem), antimycin A (Sigma), cyclosporine A (LC Laboratories), leucinostatin A (BII NPL collection), phenformin (Sigma),

alpelisib (Selleckchem), SB2343 (Selleckchem), idelalisib (Selleckchem), SB2602 (MedKoo Biosciences), CUDC-907 (Selleckchem), and TGX-221 (Selleckchem).

MTT cell viability assay

The MTT assay was used to examine the effect of SALL4 knockdown on isogenic SNU387 cell viability. Three day after viral infection, 3000 SNU-387 cells in a volume of 200 μL were plated into 96-well plates in triplicate, and incubated for the indicated time points. On the day of analysis, 20 μL of MTT solution (5 mg/mL, Sigma) was added, after which the plates were incubated for 2 hours at 37℃ to. After removal of the medium, the purple formazan crystals formed were dissolved in 100 μL DMSO with 10 minute incubation at 37℃. The optical density (OD) of dissolved purple crystal was measured by the Safire 2 plate reader (Tecan) at a wavelength of 570 nm.

CyQUANT cell viability measurements

DNA content of plated cells was measured by application of the CyQUANT Direct Cell Proliferation Kit (Thermo Fisher Scientific) that contains a cell-permeable fluorescent DNA binding dye. Cells were plated in either 96- or 384-well black, clear bottom tissue culture plates (Greiner) and allowed to reach the appropriate confluency before the addition of the appropriate amount of CyQUANT reagent, as detailed in the manufacturer's protocol. Cells were incubated for at least 1 hr at 37°C in a humidified atmosphere of 5% CO_2, after which fluorescence readings were measured by an Infinite M1000 Microplate Reader (Tecan) within a wavelength range of 480-535 nm.

CCK-8 cell viability measurements

Cells were cultured overnight in 96-well plates with 50 μl RPMI 1640 medium (10% FBS) with 1,250 cells per well for SNU-387 Empty Vector and SNU-387 parental cells, and 750 cells per well for SNU387 TgSALL4A and B cells. Cells were grown overnight before drug treatment. Phenformin, at varying concentrations, was dissolved in culture media. 50 μl of the solution was then added to each well. After 96 hr incubation, 10 μl CCK-8 reagent (Dojindo) was added to each well. After 4 hr incubation, optical density values were determined at a wavelength of 450 nm on a SpectraMax M3 Microplate Reader (Molecular Devices).

EdU cell proliferation assay

The Click-iT Plus EdU Alexa Fluor 488 Flow Cytometry Assay (Thermo Fisher Scientific) to assess cell proliferation was carried out following the manufacturer's protocol. SNU-387 isogenic lines were seeded in a 6-well plate overnight, after which the cells were incubated with 10 μM Click-iT EdU for 3 hrs. The cells were harvested and washed with 1% BSA in PBS, and incubated with Click-iT fixative for 15 mins. After fixation, the cells were washed with 1% BSA in PBS and permeabilized in Click-iT saponin-based permeabilization and wash reagent. The click-it reaction was then performed by incubation the cells with Click-iT reaction cocktail for 30 mins to label the EdU-incorporated cells with Alexa Fluor 488 dye. A standard flow cytometry method was used for determining the percentage of S-phase cells in the population using the BD LSR II Cell Analyzer (BD Biosciences).

Cell counts

SNU-387 isogenic cell lines growing at exponential phase were seeded in 6-well plates at a density of 1.5 x 10^5 cells/well. Every 3-4 days, the cells were trypsinized, after which cell

numbers were counted to record the growth of the cells. Then the cells were plated at equal cell number in new plates with fresh medium. Total cell number is presented as viable cells per well after split-adjustment.

SALL4 knockdown by lentiviral transduction

The published lenti shRNA vector pLL3.7 for scrambled (sh-scr), shSALL4-1 and shSALL4-2[3] were transfected into 293FT cells along with packaging plasmid (psPAX2) and envelope plasmid (pMD2.G) using jetPRIME® DNA transfection reagent (Polyplus-transfection® SA) according to the manufacturer's protocol for viral packaging. Viral supernatants were collected twice at 48 hrs and 72 hrs after transfection, and filtered through 0.45 μm sterile filters. Virus stocks were concentrated by ultra-centrifuge at 21,000 g for 2 hrs at 4°C. Viral transduction were carried out using spinoculation. Briefly, fresh medium containing lentivirus and 5 μg/mL Polybrene were added to plated cells. The plates was then centrifuged at 800 g at 37 °C for 1 hr, and incubated at 37°C in a humidified atmosphere of 5% CO_2.

Scrambled:
GGGTACGGTCAGGCAGCTTCTTTCAAGAGAAGAAGCTGCCTGACCGTACCCTTTTTTC
shSALL4-1:
GGCCTTGAAACAAGCCAAGCTATTCAAGAGATAGCTTGGCTTGTTTCAAGGCCTTTTTC
shSALL4-2:
TGCTATTTAGCCAAAGGCAAATTCAAGAGATTTGCCTTTGGCTAAATAGCTTTTTTC

Immunohistochemistry

Immunohistochemistry was performed using Santa Cruz SALL4 antibody (sc-101147). Slides were first deparafinized with xylene, 100% ethanol, 95% ethanol, 70% ethanol and distilled water respectively. After deparafinizing, slides were then blocked for 30 mins in blocking buffer (65 ml 100% methanol, 3.5 ml 30% hydrogen peroxide, 31.5 ml water) to block endogenous peroxidase. Subsequently, antigen retrieval was conducted in 1x pH6 citrate buffer (Sigma Aldrich) and boiled for 30 mins. Slides were washed 3 times with distilled water and blocked in normal blocking serum provided by Vectastain ABC kit for 1 hour in room temperature. Next, slides were then incubated in SALL4 primary antibody diluted 1:400 in blocking serum for 1 hour in room temperature. Prior to staining with secondary antibody, slides were washed 3 times in PBS with 0.1% triton-X. After staining with secondary antibody, slides were incubated in ABC reagent (from Vectastain ABC kit) in a humidified chamber for 1 hour in room temperature following 3 times wash in PBS. Washing was carried out in PBS for 3 times before detection was done using DAB kit (Vector laboratory) and slides were incubated in the dark at room temperature for 5 mins. Lastly, counterstaining was performed in hematoxylin for 15 mins and dehydration in 70% ethanol, 95% ethanol, 100% ethanol and xylene respectively.

Mouse Xenograft

Animals were maintained and studies were carried out according to the Institutional Animal Care and Use Committee protocols. For the SALL4-high models, the SNU-398 cell line and HCC26.1 patient primary cells were cultured as detailed in the aforementioned "Cell culture" methods. *NOD.Cg-Prkdc^{scid} Il2rg^{tm1wjl} SzJ* (NSG) mice, both male and female, were anesthetized

using 2.5% Isofluorane (Sigma). 1,000,000 cells in 200 µl of RPMI/Primary HCC cell media + Matrigel (1:1 ratio) were injected subcutaneously per mouse flank. For the SALL4-low model, the PDX1 tumor was digested with collagenase and dispase, and passed through a 70 µM strainer to obtain a sincle-cell suspension in supplemented DMEM/F12 media. The suspension was treated with red blood cell lysis buffer and DNase. After washing the cells with PBS, the suspension was mixed with an equal volume of Matrigel and injected subcutaneously in the flank of 7 female NSG mice for initial tumor propagation. The 7 PDX1 tumors were harvested after 4 weeks and processed for injection as described previously. Viable cells were counted and mixed with Matrigel to obtain a 2,500,000 cells/ml single-cell suspension. 500,000 PDX1 cells were injected subcutaneously into the left flank of each of 12 NSG mice. Isoflurane was used to anesthetize mice during injections. Drug treatment was carried out when tumors are visible. Drugs were dissolved in vehicle, 5% DMSO (Sigma) and 95% corn oil (Sigma), and injected intraperitoneal at a dose of 20 mg/kg for Sorafenib and 0.1 mg/kg for oligomycin A, with the same doses used in the combination treatment, once daily on weekdays, with no injections on weekends. Mouse weight and tumor size were recorded before each injection. Once tumors reached >1.5 cm in diameter, mice were euthanized and tumors were snap frozen in liquid nitrogen.

Mouse Toxicity Testing

Female NSG mice were injected with vehicle or 0.1 mg/kg of oligomycin A three times a week every Monday, Wednesday, and Friday for 3 weeks, then subjected to the following assays.
(1) Open field test (Locomotor testing): Mice were transported to the procedure room at least two hours prior to experiments to allow for habituation to the novel room. Locomotor activity recordings were carried out using a square open field (40x40cm) in a plexiglass cage, equipped with two rows of photocells sensitive to infrared light. The testing apparatus was enclosed in a ventilated, quiet procedure room. Measurements were performed under low levels of light to minimize stress levels of the mice, and allow for normal exploratory behavior. The mice were introduced into the locomotor cage and allowed to explore freely for 30 mins. Locomotor activity data was collected automatically. The exploratory behaviors were also captured through video recordings. The total distance travelled over 30 mins and the average velocity, from 6 independent measurements, was measured for each mouse.
(2) Grip strength tests: These tests were performed using a grip strength meter. The forelimb and full body grips of each mouse were measured in three successive trials and recorded. Hindlimb measures were calculated using the difference between the grams-force (gF) recorded for the full body and the forelimb. The results of the three tests were averaged for each mouse.
(3) Rotarod test: Mice were placed on the rotor-rod apparatus which linearly accelerated from 4 to 40 rpm at a rate of 0.1 rpm/sec. Mice were tested in four trials, with a 15 minute rest period between tests. The latency to fall and distance travelled by each mouse was recorded.
(4) Home cage recording: Each mouse was monitored in its home cage for 24 hours through video recording, to capture any instances of abnormal neurological events such as seizures.

ChIP-seq analysis

ChIP-seq data were downloaded from NCBI GEO with accession number GSE112729[4]. Reads were mapped by bowtie2 against human reference genome GRCh38. PCR duplicates were removed in the paired-end alignments by samtools rmdup[5]. Peak calling was performed by macs2 with default options. Annotation of the peaks was done by annotatePeaks.pl in Homer

software packages. Alignment files in BAM format were converted to signals by using bedtools[6], and the average coverage of each ChIP-seq experiment was adjusted to 1. bedGraphToBigWig was used to convert the result into bigWig format files. Heatmaps were generated by Deeptools2 along regions on mitochondria genes[7]. Regions were sorted according to the strength of SALL4 signals.

RNA-seq

SALL4-targeting shRNA was transduced into SNU-398 hepatocellular carcinoma (HCC) cell line as previously described[3]. Three days after transduction, the cytoplasm of the cells was removed by dounce homogenizer and nuclear RNA was extracted using the RNeasy Mini Kit (Qiagen). For SNU-387 SALL4A and SALL4B-expressing isogenic cell lines, SNU-387 HCC cells were transduced with SALL4A or SALL4B FUW-Luc-mCh-puro lentiviral constructs[8]. Puromycin was used to select for stable SALL4A or SALL4B-expressing cells. More than two weeks after selection, RNA was harvested from these isogenic cells using RNeasy Mini Kit (Qiagen). The quality of the harvested total RNA was analyzed on Bioanalyzer prior to generation of the sequencing libraries, a RIN value of >9 from all samples were observed. cDNA library construction was then performed using the stranded ScriptSeq Complete Gold kit (Human/Mouse/Rat) (Epicenter; now available through Illumina). Ribosomal RNA depletion was included in the library construction steps. Paired end 76bp sequencing was done using the Illumina HiSeq 2000 sequencer. The paired-end RNA-seq reads were mapped by TopHat2 pipeline against human reference genome GRCh38 with gene annotation GENCODE 24[9]. PCR duplicates were removed in the paired-end alignments by samtools rmdup[5]. Alignments with mapping quality < 20 were also removed. Based on the reads mapped in the transcriptome, gene expression levels in FPKM were determined by cuffdiff in the Cufflinks package[10]. GSEA analysis was preformed following the manual of the GSEA software[11]. Sequencing data has been deposited in the NCBI Gene Expression Omnibus database with accession number GSE114808.

Immunofluorescence assay and image analysis

Cells were plated in 96-well black, clear-bottom plates overnight at 50-80% confluency. The following day, MitoTracker Red CMXRos (300nM, Thermo Fisher Scientific) was added into live cells for 30 minutes at 37°C. Cells were then washed three times for 5 mins in PBS and fixed in 4% PFA for 15 mins at room temperature. Following 3 washes of PBS, cells were then incubated in blocking buffer (5% horse serum, 1% BSA, 0.2% Triton-X in PBS) for 1h at room temperature. Cytochrome-c antibody (BD Pharmigen, clone 6H2.B4) was added at 1:1000 dilution in blocking buffer and incubated overnight at 4°C. The next day, cells were washed three times for 5 mins in PBS and incubated with Alexa-Fluor-488 conjugated anti-mouse antibody (Life Technologies) at 1:400 dilution in blocking buffer for 1h at room temperature. Nuclei were stained with DAPI in blocking buffer. Imaging and quantification of relative intensities of fluorescence signals were performed with the Cytation 5 multi-mode reader and Gen5 software (BioTek).

Targeted mass spectrometry

Samples were re-suspended using 20 µL HPLC grade water for mass spectrometry. 5 µL were injected and analyzed using a hybrid 5500 QTRAP triple quadrupole mass spectrometer (AB/SCIEX) coupled to a Prominence UFLC HPLC system (Shimadzu) via selected reaction monitoring (SRM) of a total of 256 endogenous water soluble metabolites for steady-state

analyses of sample[12]. Some metabolites were targeted in both positive and negative ion mode for a total of 289 SRM transitions using positive/negative ion polarity switching. ESI voltage was +4900 V in positive ion mode and –4500 V in negative ion mode. The dwell time was 3 ms per SRM transition and the total cycle time was 1.55 seconds. Approximately 10-14 data points were acquired per detected metabolite. Samples were delivered to the mass spectrometer via hydrophilic interaction chromatography (HILIC) using a 4.6 mm i.d x 10 cm Amide XBridge column (Waters) at 400 µL/min. Gradients were run starting from 85% buffer B (HPLC grade acetonitrile) to 42% B from 0-5 minutes; 42% B to 0% B from 5-16 minutes; 0% B was held from 16-24 minutes; 0% B to 85% B from 24-25 minutes; 85% B was held for 7 minutes to re-equilibrate the column. Buffer A was comprised of 20 mM ammonium hydroxide/20 mM ammonium acetate (pH=9.0) in 95:5 water:acetonitrile. Peak areas from the total ion current for each metabolite SRM transition were integrated using MultiQuant v2.0 software (AB/SCIEX).

Metabolite profile analyses

Relative intensities of metabolites were normalized to cell number. Metabolite Set Enrichment Analysis (MSEA) was performed on the MetaboAnalyst web server with lists of metabolites with fold change more than or equal to 1.3 either up or down in the isogenic SALL4 expression cell lines compared to empty vector control, with Student's two-tailed t-test p-value of less than 0.05[13].

L-lactate cellular measurements

The L-lactate Assay kit (Abcam) was used to measure cellular lactate levels. 2.2 x 10^6 cells were washed in ice-cold PBS twice, then lysed in 220 µL of assay buffer to achieve a concentration of 10,000 cells per µL. Lysates were then spun down at 13,000 rpm for 5 mins at 4°C to pellet insoluble debris. Soluble fractions were then filtered through >30 kDa centrifugal filter units (Amicon), spun at 14,000 rpm for 20 mins at 4°C, to remove endogenous lactate dehydrogenase subunits (35 kDa) from the lysates. The assay was then performed according to the manufacturer's protocol with 50 µL of lysate (500,000 cells) per well in a 96-well plate, and the inclusion of L-lactate standards to plot a standard curve for lactate quantification.

Oxygen consumption rate and glycolysis stress test measurements

Cells were harvested and plated in the Seahorse XFe96 96-well miniplates (Agilent) coated with collagen. Cell numbers plated were 15,000 for SNU-387, SNU-387 Empty Vector, *Tg:SALL4A* and *Tg:SALL4B* cell lines, 25,000 for SNU-398 and SNU-398 sh-scr cell lines, 35,000 for the SNU-398 shSALL4-1 knockdown cell line, and 40,000 for the SNU-398 shSALL4-2 knockdown cell line. After overnight incubation, cells were washed and media was replaced with the recommended Seahorse Mitostress DMEM media and placed in a CO2-free 37°C incubator for 1 hr. Basal oxygen consumption was then measured by the Seahorse XFe96 Analyzer (Agilent) according to the manufacturer's recommended protocol. The Glycolysis Stress Test was also performed on the isogenic SALL4 expressing cell lines, prepared as described above, according to the manufacturer's recommended protocol. Cells were also subjected to the CyQUANT DNA quantification assay (Thermo Fisher Scientific) to measure DNA content, serving as a basis to normalize oxygen consumption rates with respect to cell number.

RNA/DNA extraction & quantitative RT-PCR analysis

RNA isolation was performed using the RNeasy Plus Mini Kit (Qiagen). Genomic/mitochondrial DNA isolation was performed using the QIAamp DNA Mini Kit (Qiagen). cDNA was synthesized from purified RNA with the High Capacity cDNA Reverse Transcription Kit (Applied Biosystems). Quantitative PCR for cDNA or genomic/mitochondrial DNA was performed on the ViiA 7 Real-Time PCR system (ThermoFisher Scientific) using the PowerUP SYBR Green Master Mix (Applied Biosystems). The ΔΔCt method was used for relative quantification. RT-PCR primers are:
18S rRNA forward: 5'- GTAACCCGTTGAACCCCATT -3'
18S rRNA reverse: 5'- CCATCCAATCGGTAGTAGCG -3'
ACTB forward: 5'- CAGAGCCTCGCCTTTGCCGATC -3'
ACTB reverse: 5'- CATCCATGGTGAGCTGGCGGCG -3'
ARG2 forward: 5'- CGCGAGTGCATTCCATCCT -3'
ARG2 reverse: 5'- TCCAAAGTCTTTTAGGTGGCAG -3'
B2M forward: 5'- CACTGAAAAAGATGAGTATGCC -3'
B2M reverse: 5'- AACATTCCCTGACAATCCC -3'
CLYBL forward: 5'- TCCCCAGACTTGGATATAGTTCC -3'
CLYBL reverse: 5'- TGCACAATCTACATTCAGGGATG -3'
MinorArc forward: 5'- CTAAATAGCCCACACGTTCCC -3'
MinorArc reverse: 5'- AGAGCTCCCGTGAGTGGTTA -3'
MRPL24 forward: 5'- GCCAGGTCAAACTTGTGGAT -3'
MRPL24 reverse: 5'- CCCTGATCGTGTGGAGACTC -3'
ND1 forward: 5'- ACGCCATAAAACTCTTCACCAAAG -3'
ND1 reverse: 5'- GGGTTCATAGTAGAAGAGCGATGG -3'
ND4 forward: 5'- ACCTTGGCTATCATCACCCGAT -3'
ND4 reverse: 5'- AGTGCGATGAGTAGGGGAAGG -3'
NRF1 forward: 5'- AGGAACACGGAGTGACCCAA -3'
NRF1 reverse: 5'- TGCATGTGCTTCTATGGTAGC -3'
NRF2 forward: 5'- AAGTGACAAGATGGGCTGCT -3'
NRF2 reverse: 5'- TGGACCACTGTATGGGATCA -3'
PGC-1α forward: 5'- CAAGCCAAACCAACAACTTTATCTCT -3'
PGC-1α reverse: 5'- CACACTTAAGGTGCGTTCAATAGTC -3'
PGC-1β forward: 5'- GGCAGGTTCAACCCCGA -3'
PGC-1β reverse: 5'- CTTGCTAACATCACAGAGGATATCTTG -3'
SALL4 forward: 5'- GCGAGCTTTTACCACCAAAG -3'
SALL4 reverse: 5'- CACAACAGGGTCCACATTCA -3'
SALL4A forward: 5'- TCCCCAGACTTGGATATAGTTCC -3'
SALL4A reverse: 5'- TGCACAATCTACATTCAGGGATG -3'
SALL4B forward: 5'- GGTGGATGTCAAACCCAAAG -3'
SALL4B reverse: 5'- ATGTGCCAGGAACTTCAACC
SLC25A10 forward: 5'- GTGTCGCGCTGGTACTTC -3'
SLC25A10 reverse: 5'- CACCTCCTGCTGCGTCTG -3'
SUMO1 forward: 5'- TTGGAACACCCTGTCTTTGAC -3'
SUMO1 reverse: 5'- ACCGTCATCATGTCTGACCA -3'
TFAM forward: 5'- CCGAGGTGGTTTTCATCTGT -3'
TFAM reverse: 5'- ACGCTGGGCAATTCTTCTAA -3'

Supplemental Figures/Tables:

Fig. S1. SALL4 isogenic cell lines are dependent on SALL4 for cell viability.

Fig. S2. Natural product and small molecule screening hits.

Fig. S3. Oligomycin A suppresses SALL4-dependent tumorigenesis.

Fig. S4. SALL4 expression upregulates oxidative phosphorylation gene expression.

Fig. S5. Oxidative phosphorylation and glycolysis metabolite changes induced by SALL4 expression

Fig. S6. PI3K and mTOR inhibitors have limited selectivity for SALL4 expressing cells

Fig. S7. SALL4 does not directly regulate the Urea cycle and increases mtDNA copy number

Table S1. Oxidative phosphorylation inhibitors are potent and selective against SALL4-expressing cancer cells.

Table S2. SALL4 binds a significant number of mitochondrial genes.

Table S3. SALL4 upregulates oxidative phosphorylation gene expression by RNA-seq GSEA.

Fig. S1. SALL4 isogenic cell lines are dependent on SALL4 for cell viability. (**A**) *SALL4* mRNA expression in *SALL4* endogenous cell lines used in the screen, measured by qRT-PCR and normalized to *ACTB* (mean of 4 replicates ± SD). (**B**) *SALL4* mRNA expression in SNU-387 isogenic empty vector, *SALL4A*, and *SALL4B* expressing cell lines used in the screen, measured by qRT-PCR and normalized to *ACTB* (mean of 2 replicates ± SD). (**C**) Western blot of SALL4 protein in the *SALL4* endogenous cell lines, with ACTB loading control. Bands were quantified by densitometry with SNU-387 bands as reference. (**D**) Western blot of SALL4 protein isoforms and *SALL4* knockdown validation in the isogenic cell lines, with ACTB loading control. Bands were quantified by densitometry with sh-scr bands as reference. (**E**) MTT oxidoreductase-dependent cell viability assay on *SALL4* isogenic cell lines with *SALL4* knockdown, normalized to day 5 sh-scr scrambled control (mean of 3 replicates ± SD). (**F**) Cell counts of SALL4-expressing isogenic cell lines over 10 days (mean of 3 replicates ± SD). (**G**) EdU incorporation, during DNA synthesis, measurements for the percentage of EdU labeled cells after 3 hrs of treatment for the SALL4-expressing isogenic cell lines (performed in singlet).

Fig. S2. Natural product and small molecule screening hits. (**A**) Cell viability fold change plots of control compounds obtained from the pilot screen and used for the complete screen, measured with CellTiter-Glo cell viability reagent, and normalized to DMSO-treated cell viability (mean of 3 replicates ± SD). (**B**) Cell viability dose-response curves for cells treated for 96 hrs with synthetic compound hit PI-103, measured with CellTiter-Glo and CyQUANT reagents and normalized to untreated cell viability (mean of 3 replicates ± SD). (**C**) Cell viability dose-response curves for cells treated for 96 hrs with hit compounds from the natural product extract screen, oligomycin, efrapeptin, antimycin, and leucinostatin, measured with CyQUANT reagent and normalized to untreated cell viability (mean of 3 replicates ± SD). (**D**) Western blot for apoptosis marker cleaved caspase-3 and control total caspase-3 protein levels in oligomycin A-treated SNU-398 cells. Bands were quantified by densitometry with DMSO bands as reference.

Fig. S3. Oligomycin A suppresses SALL4-dependent tumorigenesis. (**A**) *SALL4* mRNA expression in HCC cell lines with respect to immortalized normal liver cell line THLE-3 *SALL4* transcript levels, measured by qRT-PCR and normalized to *18S* rRNA (mean of 3 replicates ± SD). Oligomycin A IC_{50} values from dose response curves in Fig. 3A are detailed above the bar graphs for corresponding cell lines. (**B**) *SALL4* mRNA expression in a pair of $SALL4^{hi}$ and $SALL4^{lo}$ NSCLC cell lines with respect to immortalized normal liver cell line THLE-3 *SALL4* transcript levels, measured by qRT-PCR and normalized to *18S* rRNA (mean of 2 replicates ± SD). Oligomycin A IC_{50} values from dose response curves in Fig. S3C are detailed above the bar graphs for corresponding cell lines. (**C**) Cell viability dose-response curves for lung cancer cell lines in (**B**) treated with oligomycin A, measured with CellTiter-Glo reagent and normalized to untreated cell viability (mean of 3 replicates ± SD). (**D**) Tumor images from the SNU-398 mouse xenograft experiment in Fig. 3B. (**D**) Tumor images from the SNU-398 mouse xenograft experiment in Fig. 3C. (**E**) Tumor images from the HCC26.1 mouse patient-derived xenograft experiment in Fig. 3E. (**F**) SALL4 immunohistochemistry on a PDX1 tumor section and a SALL4 positive control tumor section. (**G**) Tumor images from the PDX1 mouse patient-derived xenograft experiment in Fig. 3G. Four tumors were excised on day 32 as their size reached the designated animal protocol endpoint while the remaining mice continued drug treatment till day 36, when all remaining tumors reached the endpoint. (**H**) Open field test conducted on mice injected with vehicle (n=6) and 0.1 mg/kg oligomycin A (n=6) over 3 weeks (mean ± SD). (**I**) Grip strength test conducted on the mice in (**H**) (mean ± SD). (**J**) Rotarod test conducted on the mice in (**H**) (mean ± SD). (**K**) HCC patient stratification by SALL4 expression and diabetics. Numbers above bar graphs indicate absolute patient numbers. (**L**) Cell viability dose-response curves for cells treated for 96 hrs with phenformin or oligomycin A, measured with CCK-8 dehydrogenase activity assay and normalized to untreated cell viability (mean of 3 replicates ± SD).

Fig. S4. SALL4 expression upregulates oxidative phosphorylation gene expression. (**A**) RNA-seq expression level fold change for SALL4, in the SNU-398 *SALL4* knockdown and isogenic *SALL4* expressing cell lines, normalized respectively to expression levels in the SNU-398 input and SNU-387 empty vector control cell line, performed in singlet. (**B**) RNA-seq expression level fold change for a panel of mitochondrial genes from Fig. 4D with *SALL4* knockdown in the SNU-398 cells, normalized to expression levels in the SNU-398 control, performed in singlet. (**C**) mRNA expression validation of selected mitochondrial genes in the *SALL4* expressing isogenic cell lines used in the screen, measured by qRT-PCR and normalized to *18S* rRNA (mean of 3 replicates ± SD). (**D**) mRNA expression validation of the mitochondrial genes from (**C**) with *SALL4* knockdown for 72 hrs in the SNU-398 cell line, measured by qRT-PCR and normalized to *18S* rRNA (mean of 2 replicates ± SD). (**E**) GSEA plots for oxidative phosphorylation from analysis of the RNA-seq data set in (**A**). (**F**) Western blots for SALL4-bound mitochondrial genes and ACTB loading control in the cell lines used in the screen. Bands were quantified by densitometry with SNU-387 and EV bands as references. (**G**) Western blots for the genes in (**F**) in the SNU-398 cell line 72 hours after *SALL4* knockdown. Bands were quantified by densitometry with sh-scr bands as reference.

Fig. S5. Oxidative phosphorylation and glycolysis metabolite changes induced by SALL expression. (**A**) Metabolite Set Enrichment Analysis (MSEA) of significantly altered metabolites (1.3 fold change, $P < 0.05$) in the SNU-387 *Tg:SALL4A* cells compared to empty

vector control. (**B**) MSEA of significantly altered metabolites (1.3 fold change, $P < 0.05$) in the SNU-387 *Tg:SALL4B* cells compared to empty vector control. (**C**) Fold change of malate-aspartate shuttle metabolites in the SALL4-expressing isogenic lines normalized to empty vector control (mean of 3 replicates ± SD). (**D**) Fold change of glycolytic metabolites in the SALL4-expressing isogenic lines normalized to empty vector control (mean of 3 replicates ± SD). (**E**) L-lactate measurements, utilizing a lactate dehydrogenase enzymatic assay, in the SALL4 isogenic cell lines and no enzyme controls, normalized by cell number (mean of 2 replicates ± SD). (**F**) Extracellular acidification rate (ECAR) measurements per DNA content in the SALL4 isogenic lines, normalized to CyQUANT DNA quantification reagent values (mean of 3 replicates ± SD). (**G**) Glycolysis stress test assessing ECAR when cells are treated with glucose post starvation, ATP synthase inhibitor oligomycin, and glycolysis inhibitor 2-Deoxy-D-glucose that quantifies glycolytic flux and glycolytic capacity, performed on the SALL4-expressing isogenic lines (mean of 3 replicates ± SD).

Fig. S6. PI3K and mTOR inhibitor have limited selectivity for SALL4 expressing cells. (**A**) Cell viability dose-response curves for cells treated for 72 hrs with selective PI3K or mTOR inhibitors alpelisib, SB2343, idelalisib, SB2602, CUDC-907, and TGX-221 measured with CellTiter-Glo reagent and normalized to DMSO-treated cell viability (mean of 3 replicates ± SD).

Fig. S7. SALL4 does not directly regulate the Urea cycle and increases mtDNA copy number. (**A**) Fold change of urea cycle metabolites in the SALL4-expressing isogenic lines normalized to empty vector control (mean of 3 replicates ± SD). (**B**) Representative ChIP-seq input, H3K27ac, and SALL4 peaks for urea cycle genes. (**C**) mtDNA quantification with primers to the Minor Arc, *ND1* and *ND4* genes in *SALL4* endogenous and isogenic cell lines used in the screen, measured by qRT-PCR and normalized to *B2M* (mean of 3 replicates ± SD). (**D**) mRNA expression of mitochondrial biogenesis genes in the *SALL4* expressing isogenic cell lines used in the screen, measured by qRT-PCR and normalized to *18S* rRNA (mean of 3 replicates ± SD). (**E**) Representative ChIP-seq input, H3K27ac, and SALL4 peaks for the mitochondrial biogenesis genes in (**D**).

Table S1. Oxidative phosphorylation inhibitors are potent and selective against SALL4-expressing cancer cells. (**A**) Summary of IC_{50} and selectivity values for oxidative phosphorylation inhibitors tested in the SALL4 endogenous HCC cell lines used in the screen. (**B**) Summary of IC_{50} and selectivity values for oxidative phosphorylation inhibitors tested in the SALL4 endogenous NSCLC cell line pair in Fig. S3C.

Table S2. SALL4 binds a significant number of mitochondrial genes. (**A**) List of mitochondrial genes bound by SALL4 from previously published SNU-398 ChIP-seq experiments.

Table S3. SALL4 upregulates oxidative phosphorylation gene expression by RNA-seq GSEA. (**A**) Gene sets upregulated in the SNU-398 input sample compared to SNU-398 shSALL4-1 knockdown. (**B**) Gene sets upregulated in the SNU-398 shSALL4-1 knockdown sample compared to SNU-398 input. (**C**) Gene sets upregulated in the SNU-387 Empty Vector cell line compared to SNU-387 *Tg:SALL4A*. (**D**) Gene sets upregulated in the SNU-387

Tg:SALL4A cell line compared to SNU-387 Empty Vector. (**E**) Gene sets upregulated in the SNU-387 Empty Vector cell line compared to SNU-387 *Tg:SALL4B*. (**F**) Gene sets upregulated in the SNU-387 *Tg:SALL4B* cell line compared to SNU-387 Empty Vector.

Supplemental References:

1. Butler MS, Yoganathan K, Buss AD, et al. Identification of aluminium dioxalate in fungal cultures grown on vermiculite. J Antibiot (Tokyo) 2012;65:275–276.

2. Boot CM, Tenney K, Valeriote FA, et al. Highly N-Methylated Linear Peptides Produced by an Atypical Sponge-Derived Acremonium sp. J Nat Prod 2006;69:83–92.

3. Yong KJ, Gao C, Lim JSJ, et al. Oncofetal gene SALL4 in aggressive hepatocellular carcinoma. N Engl J Med 2013;368:2266–2276.

4. **Liu BH**, **Jobichen C**, Chia CSB, et al. Targeting cancer addiction for SALL4 by shifting its transcriptome with a pharmacologic peptide. Proc Natl Acad Sci U S A 2018;115:E7119–E7128.

5. **Li H**, **Handsaker B**, Wysoker A, et al. The Sequence Alignment/Map format and SAMtools. Bioinforma Oxf Engl 2009;25:2078–2079.

6. Quinlan AR, Hall IM. BEDTools: a flexible suite of utilities for comparing genomic features. Bioinforma Oxf Engl 2010;26:841–842.

7. **Ramírez F**, **Ryan DP**, Grüning B, et al. deepTools2: a next generation web server for deep-sequencing data analysis. Nucleic Acids Res 2016;44:W160-165.

8. Li A, Jiao Y, Yong KJ, et al. SALL4 is a new target in endometrial cancer. Oncogene 2015;34:63–72.

9. Kim D, Pertea G, Trapnell C, et al. TopHat2: accurate alignment of transcriptomes in the presence of insertions, deletions and gene fusions. Genome Biol 2013;14:R36.

10. Trapnell C, Roberts A, Goff L, et al. Differential gene and transcript expression analysis of RNA-seq experiments with TopHat and Cufflinks. Nat Protoc 2012;7:562–578.

11. **Subramanian A**, **Tamayo P**, Mootha VK, et al. Gene set enrichment analysis: a knowledge-based approach for interpreting genome-wide expression profiles. Proc Natl Acad Sci U S A 2005;102:15545–15550.

12. **Yuan M**, **Breitkopf SB**, Yang X, et al. A positive/negative ion-switching, targeted mass spectrometry-based metabolomics platform for bodily fluids, cells, and fresh and fixed tissue. Nat Protoc 2012;7:872–881.

13. Xia J, Wishart DS. MSEA: a web-based tool to identify biologically meaningful patterns in quantitative metabolomic data. Nucleic Acids Res 2010;38:W71-77.

Author names in bold designate shared co-first authorship.

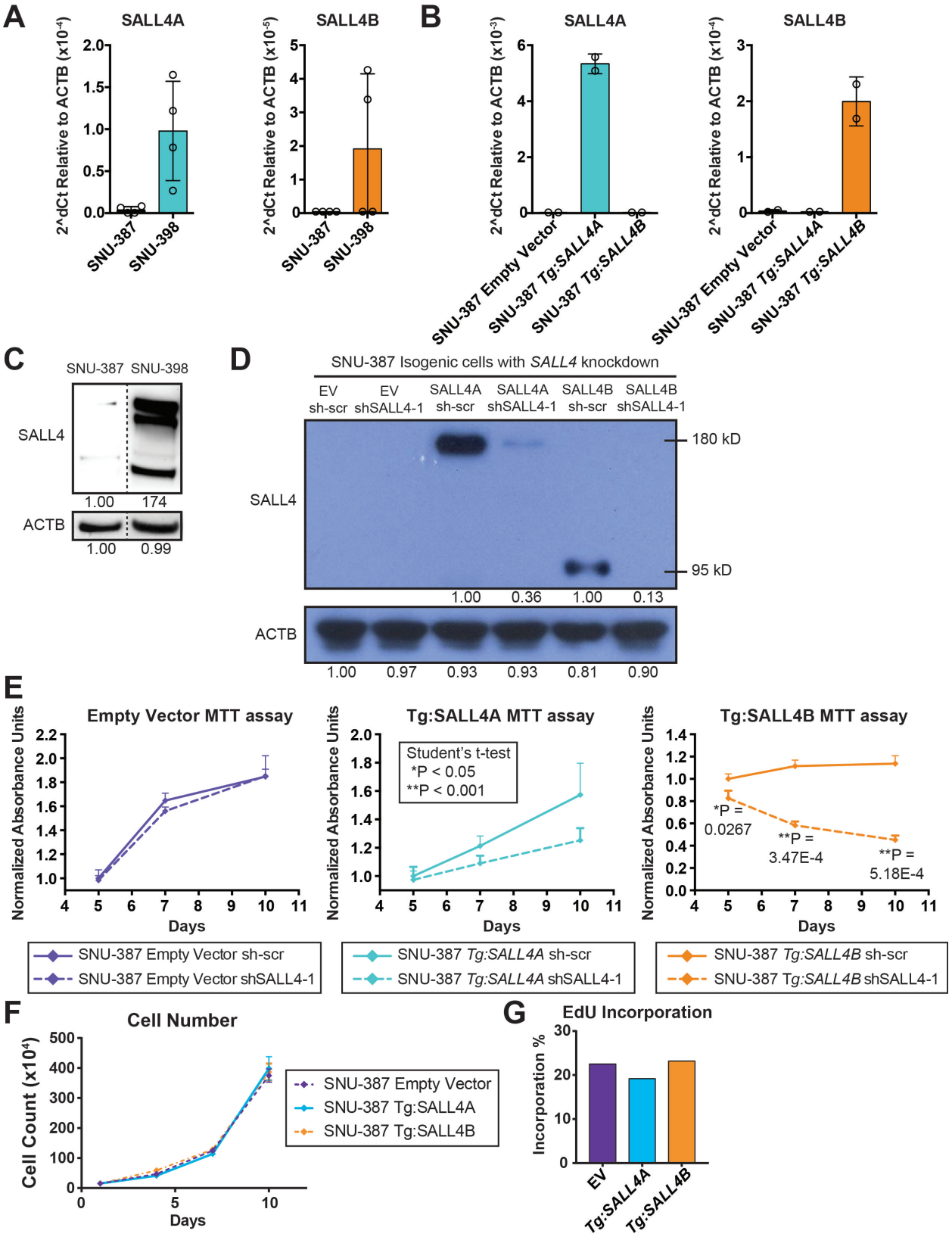
A
SALL4A
2^-dCt Relative to ACTB (x10⁻⁴)
SNU-387
SNU-398
SALL4B
2^-dCt Relative to ACTB (x10⁻⁵)
B
SALL4A
2^-dCt Relative to ACTB (x10⁻³)
SNU-387 Empty Vector
SNU-387 Tg:SALL4A
SNU-387 Tg:SALL4B
SALL4B
2^-dCt Relative to ACTB (x10⁻⁴)
C
SNU-387 SNU-398
SALL4
1.00 174
ACTB
1.00 0.99
D
SNU-387 Isogenic cells with SALL4 knockdown
EV sh-scr
EV shSALL4-1
SALL4A sh-scr
SALL4A shSALL4-1
SALL4B sh-scr
SALL4B shSALL4-1
SALL4
180 kD
95 kD
1.00 0.36 1.00 0.13
ACTB
1.00 0.97 0.93 0.93 0.81 0.90
E
Empty Vector MTT assay
Tg:SALL4A MTT assay
Tg:SALL4B MTT assay
Normalized Absorbance Units
Days
Student's t-test
*P < 0.05
**P < 0.001
*P = 0.0267
**P = 3.47E-4
**P = 5.18E-4
SNU-387 Empty Vector sh-scr
SNU-387 Empty Vector shSALL4-1
SNU-387 Tg:SALL4A sh-scr
SNU-387 Tg:SALL4A shSALL4-1
SNU-387 Tg:SALL4B sh-scr
SNU-387 Tg:SALL4B shSALL4-1
F
Cell Number
Cell Count (x10⁴)
Days
SNU-387 Empty Vector
SNU-387 Tg:SALL4A
SNU-387 Tg:SALL4B
G
EdU Incorporation
Incorporation %
EV
Tg:SALL4A
Tg:SALL4B

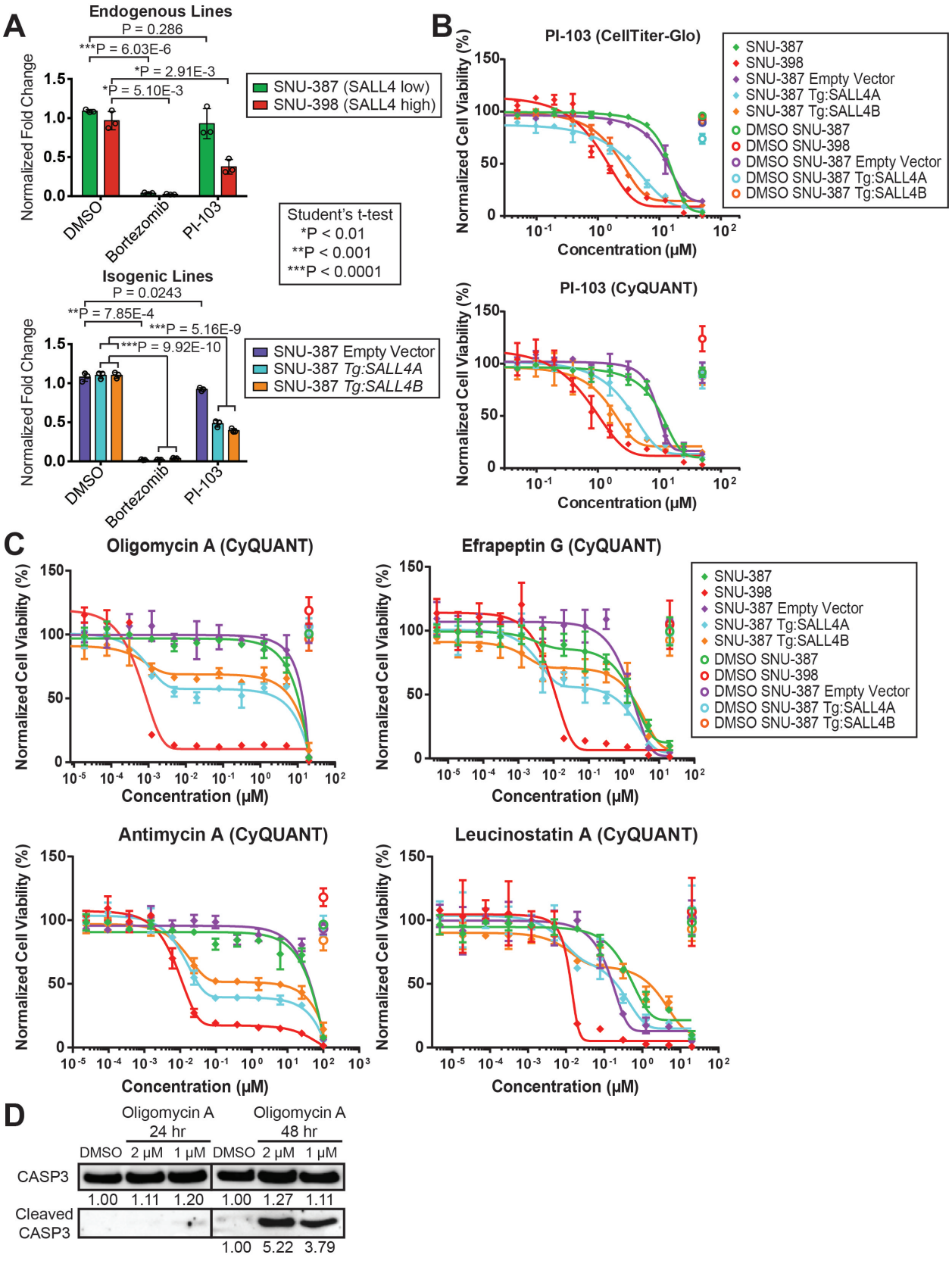
A
Endogenous Lines
P = 0.286
***P = 6.03E-6
*P = 2.91E-3
*P = 5.10E-3
Normalized Fold Change
SNU-387 (SALL4 low)
SNU-398 (SALL4 high)
DMSO
Bortezomib
PI-103
Student's t-test
*P < 0.01
**P < 0.001
***P < 0.0001
Isogenic Lines
P = 0.0243
**P = 7.85E-4
***P = 5.16E-9
***P = 9.92E-10
SNU-387 Empty Vector
SNU-387 Tg:SALL4A
SNU-387 Tg:SALL4B
B
PI-103 (CellTiter-Glo)
PI-103 (CyQUANT)
Normalized Cell Viability (%)
Concentration (μM)
SNU-387
SNU-398
SNU-387 Empty Vector
SNU-387 Tg:SALL4A
SNU-387 Tg:SALL4B
DMSO SNU-387
DMSO SNU-398
DMSO SNU-387 Empty Vector
DMSO SNU-387 Tg:SALL4A
DMSO SNU-387 Tg:SALL4B
C
Oligomycin A (CyQUANT)
Efrapeptin G (CyQUANT)
Antimycin A (CyQUANT)
Leucinostatin A (CyQUANT)
D
Oligomycin A
24 hr
48 hr
DMSO 2 μM 1 μM DMSO 2 μM 1 μM
CASP3
1.00 1.11 1.20 1.00 1.27 1.11
Cleaved CASP3
1.00 5.22 3.79

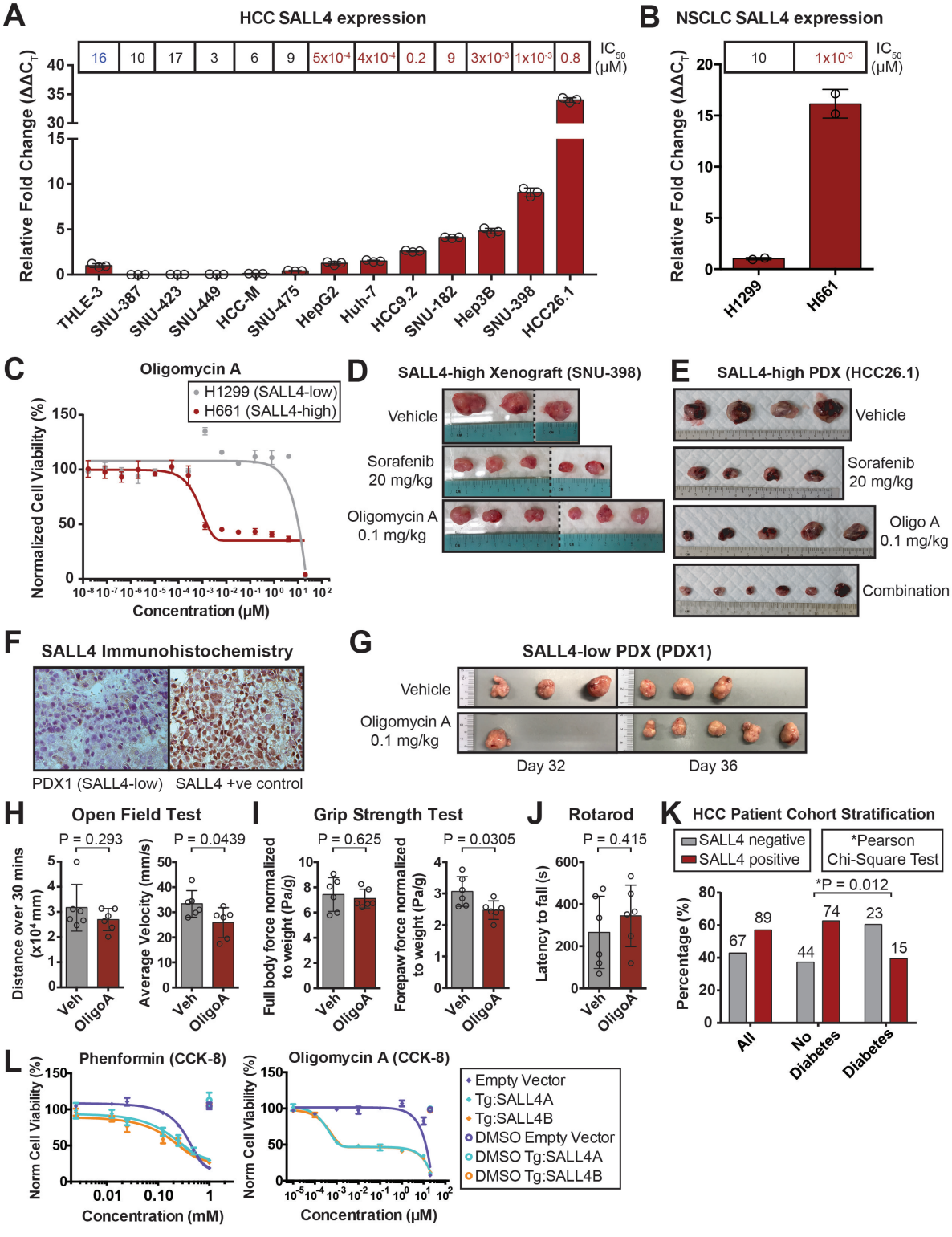
A
HCC SALL4 expression
IC50 (μM)
16
10
17
3
6
9
5x10-4
4x10-4
0.2
9
3x10-3
1x10-3
0.8
Relative Fold Change (ΔΔCT)
THLE-3
SNU-387
SNU-423
SNU-449
HCC-M
SNU-475
HepG2
Huh-7
HCC9.2
SNU-182
Hep3B
SNU-398
HCC26.1
B
NSCLC SALL4 expression
10
1x10-3
H1299
H661
C
Oligomycin A
H1299 (SALL4-low)
H661 (SALL4-high)
Normalized Cell Viability (%)
Concentration (μM)
D
SALL4-high Xenograft (SNU-398)
Vehicle
Sorafenib 20 mg/kg
Oligomycin A 0.1 mg/kg
E
SALL4-high PDX (HCC26.1)
Vehicle
Sorafenib 20 mg/kg
Oligo A 0.1 mg/kg
Combination
F
SALL4 Immunohistochemistry
PDX1 (SALL4-low)
SALL4 +ve control
G
SALL4-low PDX (PDX1)
Vehicle
Oligomycin A 0.1 mg/kg
Day 32
Day 36
H
Open Field Test
P = 0.293
P = 0.0439
Distance over 30 mins (x10⁴ mm)
Average Velocity (mm/s)
Veh
OligoA
I
Grip Strength Test
P = 0.625
P = 0.0305
Full body force normalized to weight (Pa/g)
Forepaw force normalized to weight (Pa/g)
J
Rotarod
P = 0.415
Latency to fall (s)
K
HCC Patient Cohort Stratification
SALL4 negative
SALL4 positive
*Pearson Chi-Square Test
*P = 0.012
Percentage (%)
67
89
44
74
23
15
All
No Diabetes
Diabetes
L
Phenformin (CCK-8)
Oligomycin A (CCK-8)
Norm Cell Viability (%)
Concentration (mM)
Concentration (μM)
Empty Vector
Tg:SALL4A
Tg:SALL4B
DMSO Empty Vector
DMSO Tg:SALL4A
DMSO Tg:SALL4B

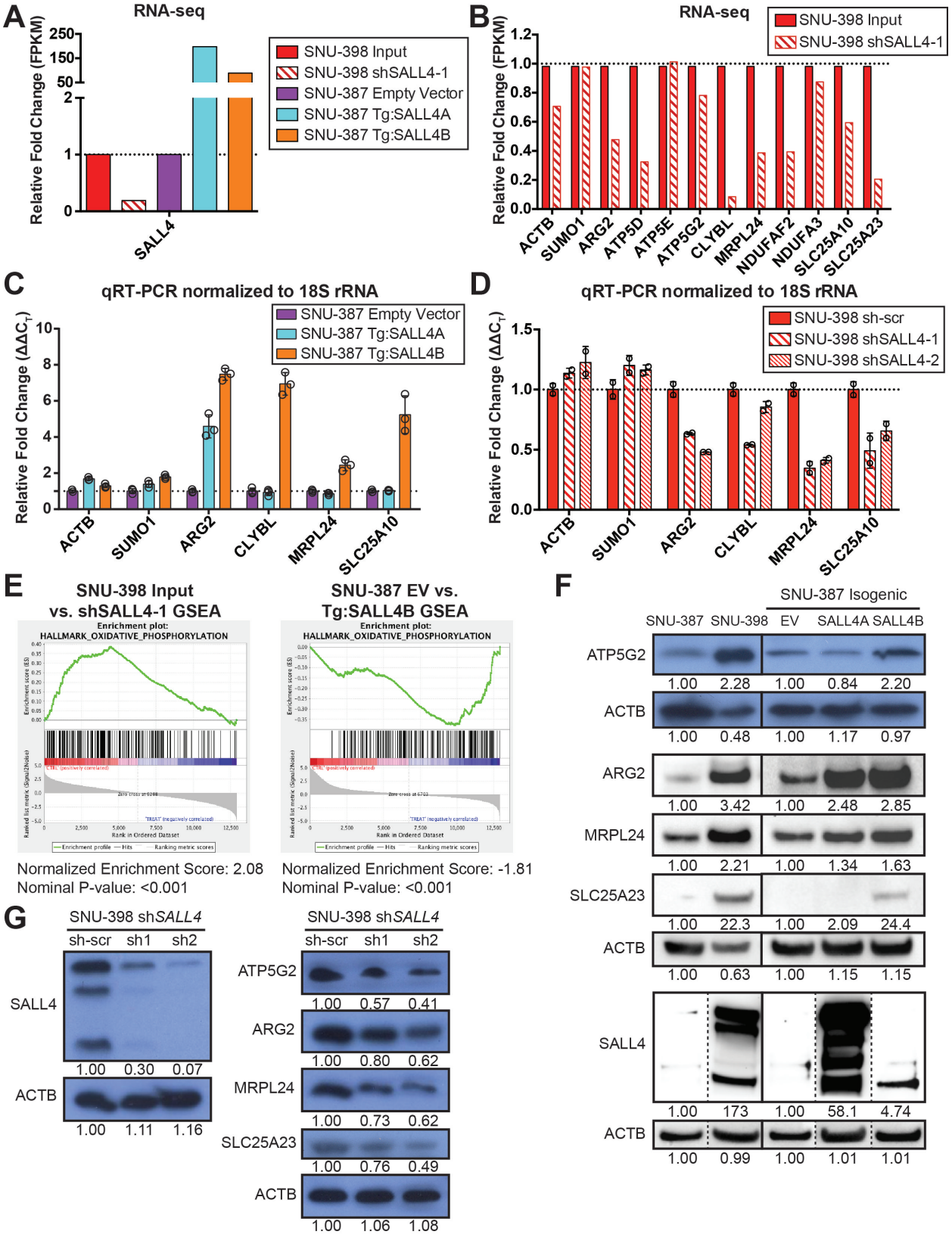
A
RNA-seq
Relative Fold Change (FPKM)
SNU-398 Input
SNU-398 shSALL4-1
SNU-387 Empty Vector
SNU-387 Tg:SALL4A
SNU-387 Tg:SALL4B
SALL4
B
RNA-seq
SNU-398 Input
SNU-398 shSALL4-1
Relative Fold Change (FPKM)
ACTB
SUMO1
ARG2
ATP5D
ATP5E
ATP5G2
CLYBL
MRPL24
NDUFAF2
NDUFA3
SLC25A10
SLC25A23
C
qRT-PCR normalized to 18S rRNA
SNU-387 Empty Vector
SNU-387 Tg:SALL4A
SNU-387 Tg:SALL4B
Relative Fold Change (ΔΔC_T)
ACTB
SUMO1
ARG2
CLYBL
MRPL24
SLC25A10
D
qRT-PCR normalized to 18S rRNA
SNU-398 sh-scr
SNU-398 shSALL4-1
SNU-398 shSALL4-2
Relative Fold Change (ΔΔC_T)
ACTB
SUMO1
ARG2
CLYBL
MRPL24
SLC25A10
E
SNU-398 Input
vs. shSALL4-1 GSEA
Enrichment plot:
HALLMARK_OXIDATIVE_PHOSPHORYLATION
Normalized Enrichment Score: 2.08
Nominal P-value: <0.001
SNU-387 EV vs.
Tg:SALL4B GSEA
Enrichment plot:
HALLMARK_OXIDATIVE_PHOSPHORYLATION
Normalized Enrichment Score: -1.81
Nominal P-value: <0.001
F
SNU-387 Isogenic
SNU-387 SNU-398 EV SALL4A SALL4B
ATP5G2
1.00 2.28 1.00 0.84 2.20
ACTB
1.00 0.48 1.00 1.17 0.97
ARG2
1.00 3.42 1.00 2.48 2.85
MRPL24
1.00 2.21 1.00 1.34 1.63
SLC25A23
1.00 22.3 1.00 2.09 24.4
ACTB
1.00 0.63 1.00 1.15 1.15
SALL4
1.00 173 1.00 58.1 4.74
ACTB
1.00 0.99 1.00 1.01 1.01
G
SNU-398 shSALL4
sh-scr sh1 sh2
SALL4
1.00 0.30 0.07
ACTB
1.00 1.11 1.16
SNU-398 shSALL4
sh-scr sh1 sh2
ATP5G2
1.00 0.57 0.41
ARG2
1.00 0.80 0.62
MRPL24
1.00 0.73 0.62
SLC25A23
1.00 0.76 0.49
ACTB
1.00 1.06 1.08

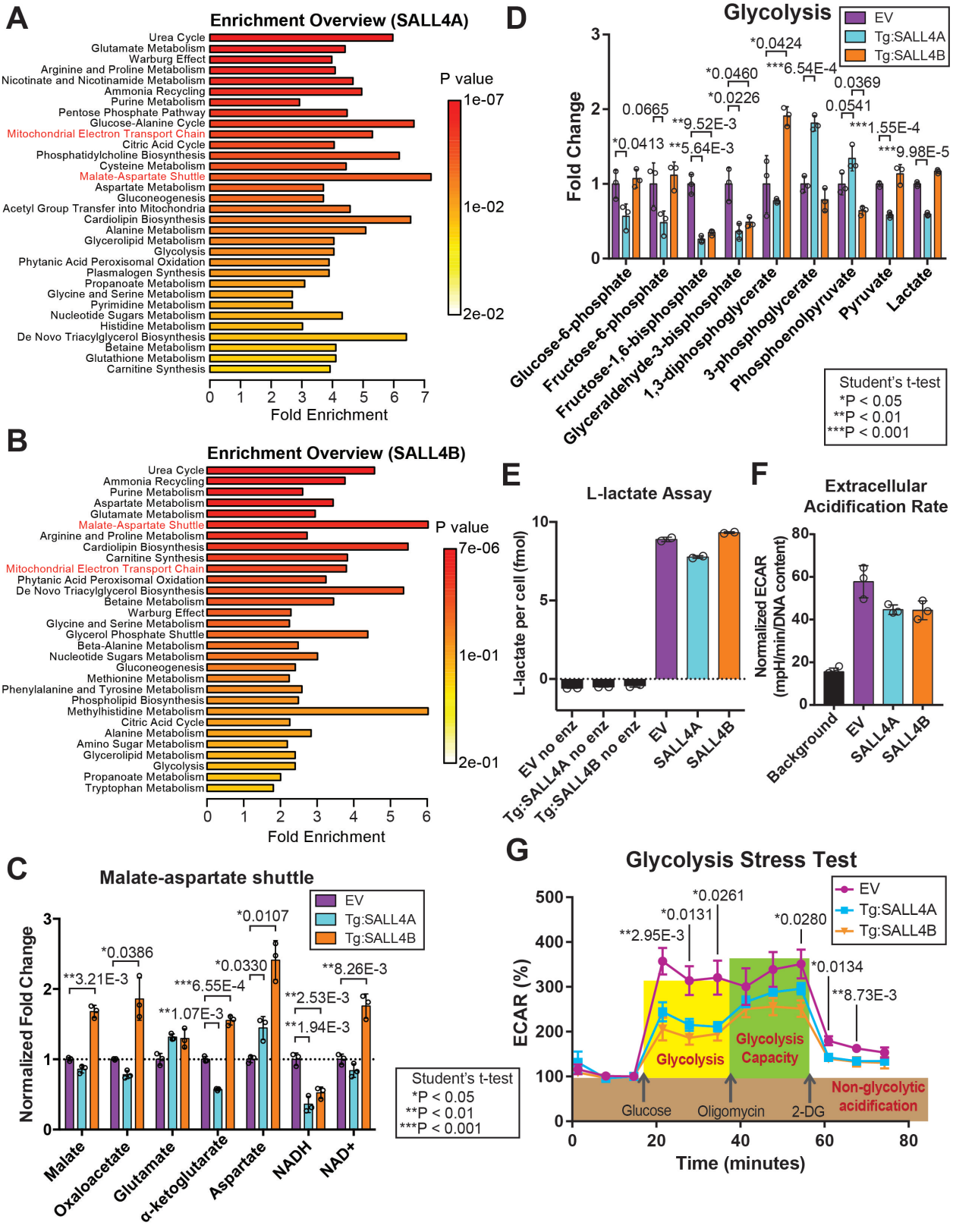
A
Enrichment Overview (SALL4A)
Urea Cycle
Glutamate Metabolism
Warburg Effect
Arginine and Proline Metabolism
Nicotinate and Nicotinamide Metabolism
Ammonia Recycling
Purine Metabolism
Pentose Phosphate Pathway
Glucose-Alanine Cycle
Mitochondrial Electron Transport Chain
Citric Acid Cycle
Phosphatidylcholine Biosynthesis
Cysteine Metabolism
Malate-Aspartate Shuttle
Aspartate Metabolism
Gluconeogenesis
Acetyl Group Transfer into Mitochondria
Cardiolipin Biosynthesis
Alanine Metabolism
Glycerolipid Metabolism
Glycolysis
Phytanic Acid Peroxisomal Oxidation
Plasmalogen Synthesis
Propanoate Metabolism
Glycine and Serine Metabolism
Pyrimidine Metabolism
Nucleotide Sugars Metabolism
Histidine Metabolism
De Novo Triacylglycerol Biosynthesis
Betaine Metabolism
Glutathione Metabolism
Carnitine Synthesis
P value
1e-07
1e-02
2e-02
0 1 2 3 4 5 6 7
Fold Enrichment
B
Enrichment Overview (SALL4B)
Urea Cycle
Ammonia Recycling
Purine Metabolism
Aspartate Metabolism
Glutamate Metabolism
Malate-Aspartate Shuttle
Arginine and Proline Metabolism
Cardiolipin Biosynthesis
Carnitine Synthesis
Mitochondrial Electron Transport Chain
Phytanic Acid Peroxisomal Oxidation
De Novo Triacylglycerol Biosynthesis
Betaine Metabolism
Warburg Effect
Glycine and Serine Metabolism
Glycerol Phosphate Shuttle
Beta-Alanine Metabolism
Nucleotide Sugars Metabolism
Gluconeogenesis
Methionine Metabolism
Phenylalanine and Tyrosine Metabolism
Phospholipid Biosynthesis
Methylhistidine Metabolism
Citric Acid Cycle
Alanine Metabolism
Amino Sugar Metabolism
Glycerolipid Metabolism
Glycolysis
Propanoate Metabolism
Tryptophan Metabolism
P value
7e-06
1e-01
2e-01
0 1 2 3 4 5 6
Fold Enrichment
C
Malate-aspartate shuttle
EV
Tg:SALL4A
Tg:SALL4B
Normalized Fold Change
**3.21E-3
*0.0386
**1.07E-3
***6.55E-4
*0.0330
*0.0107
**1.94E-3
**2.53E-3
**8.26E-3
Malate
Oxaloacetate
Glutamate
α-ketoglutarate
Aspartate
NADH
NAD+
Student's t-test
*P < 0.05
**P < 0.01
***P < 0.001
D
Glycolysis
EV
Tg:SALL4A
Tg:SALL4B
Fold Change
*0.0413
0.0665
**5.64E-3
**9.52E-3
*0.0460
*0.0226
*0.0424
***6.54E-4
0.0369
0.0541
***1.55E-4
***9.98E-5
Glucose-6-phosphate
Fructose-6-phosphate
Fructose-1,6-bisphosphate
Glyceraldehyde-3-bisphosphate
1,3-diphosphoglycerate
3-phosphoglycerate
Phosphoenolpyruvate
Pyruvate
Lactate
Student's t-test
*P < 0.05
**P < 0.01
***P < 0.001
E
L-lactate Assay
L-lactate per cell (fmol)
EV no enz
Tg:SALL4A no enz
Tg:SALL4B no enz
EV
SALL4A
SALL4B
F
Extracellular Acidification Rate
Normalized ECAR (mpH/min/DNA content)
Background
EV
SALL4A
SALL4B
G
Glycolysis Stress Test
EV
Tg:SALL4A
Tg:SALL4B
ECAR (%)
**2.95E-3
*0.0131
*0.0261
*0.0280
*0.0134
**8.73E-3
Glycolysis
Glycolysis Capacity
Non-glycolytic acidification
Glucose
Oligomycin
2-DG
Time (minutes)

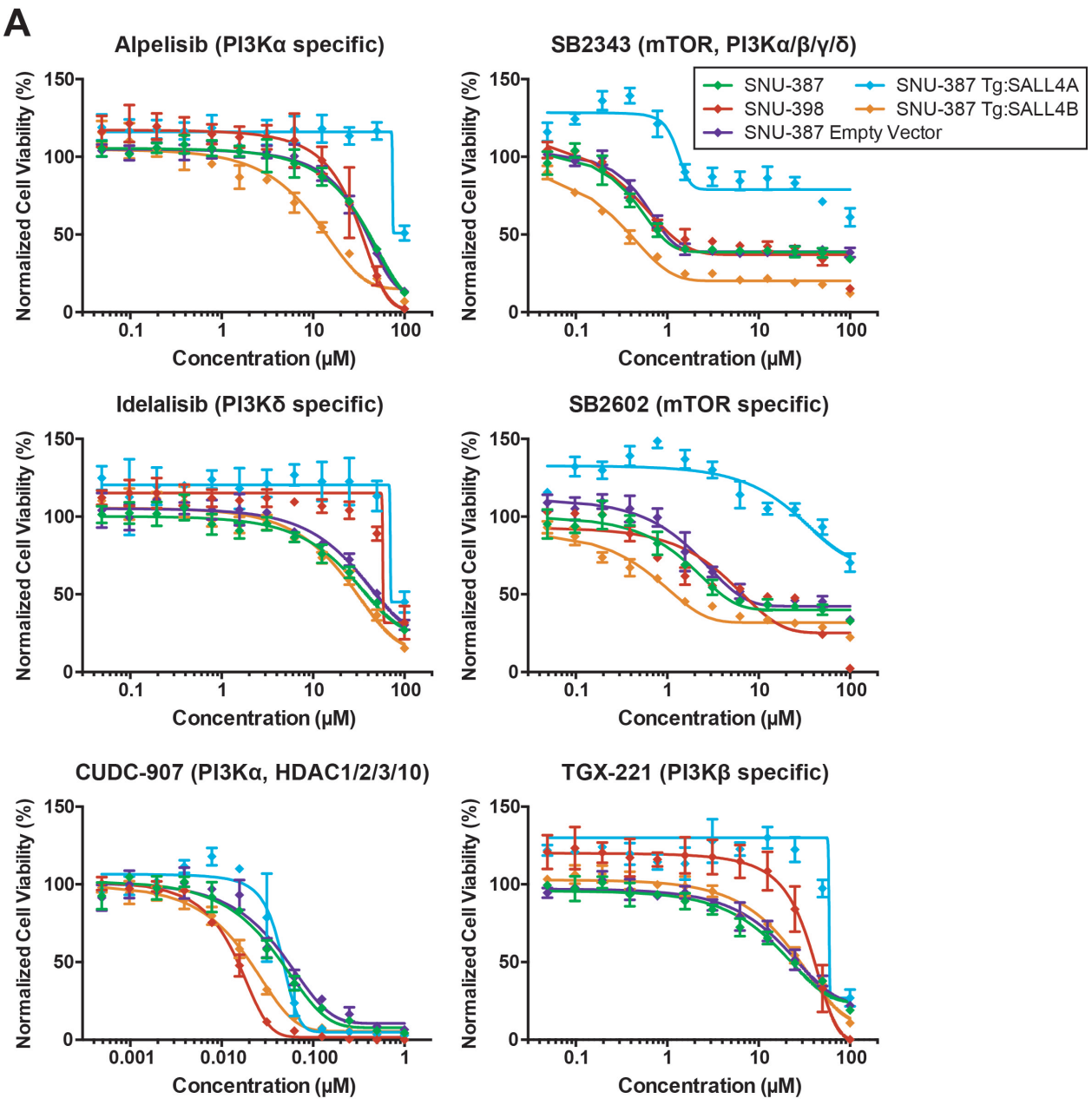
A
Alpelisib (PI3Kα specific)
SB2343 (mTOR, PI3Kα/β/γ/δ)
Idelalisib (PI3Kδ specific)
SB2602 (mTOR specific)
CUDC-907 (PI3Kα, HDAC1/2/3/10)
TGX-221 (PI3Kβ specific)
SNU-387
SNU-398
SNU-387 Empty Vector
SNU-387 Tg:SALL4A
SNU-387 Tg:SALL4B
Normalized Cell Viability (%)
Concentration (μM)
0
50
100
150
0.001
0.010
0.100
0.1
1
10
100

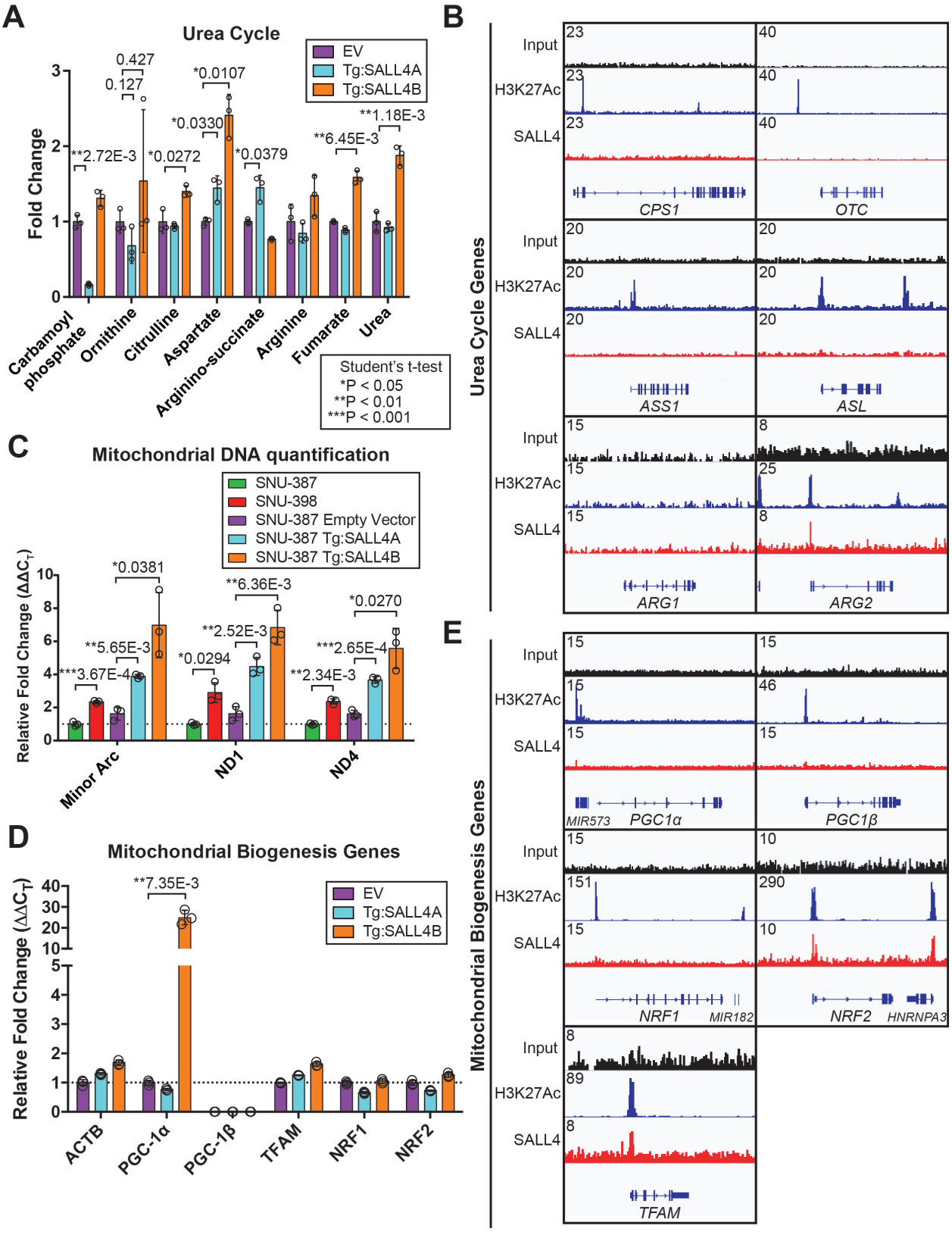
A
Urea Cycle
EV
Tg:SALL4A
Tg:SALL4B
Fold Change
0.427
0.127
*0.0107
*0.0330
**1.18E-3
**2.72E-3
*0.0272
*0.0379
**6.45E-3
Carbamoyl phosphate
Ornithine
Citrulline
Aspartate
Arginino-succinate
Arginine
Fumarate
Urea
Student's t-test
*P < 0.05
**P < 0.01
***P < 0.001
B
Urea Cycle Genes
Input
H3K27Ac
SALL4
CPS1
OTC
ASS1
ASL
ARG1
ARG2
C
Mitochondrial DNA quantification
SNU-387
SNU-398
SNU-387 Empty Vector
SNU-387 Tg:SALL4A
SNU-387 Tg:SALL4B
Relative Fold Change (ΔΔCT)
*0.0381
**6.36E-3
*0.0270
**5.65E-3
**2.52E-3
***2.65E-4
***3.67E-4
*0.0294
**2.34E-3
Minor Arc
ND1
ND4
D
Mitochondrial Biogenesis Genes
EV
Tg:SALL4A
Tg:SALL4B
Relative Fold Change (ΔΔCT)
**7.35E-3
ACTB
PGC-1α
PGC-1β
TFAM
NRF1
NRF2
E
Mitochondrial Biogenesis Genes
Input
H3K27Ac
SALL4
MIR573
PGC1α
PGC1β
NRF1
MIR182
NRF2
HNRNPA3
TFAM